Pick and place routines with a flexible joint robotic arm using passivity-based control

Anno Veltman

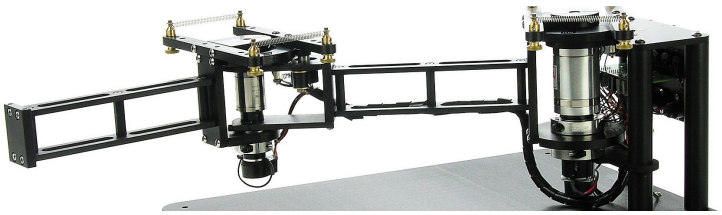

A thesis presented for the degree of
Master of Science

Industrial Engineering and Management
Faculty of Science and Engineering
University of Groningen

Supervisors

Dr. L.P. Borja Rosales

Prof. dr. ir. J.M.A. Scherpen

Prof. dr. ir. B. Jayawardhana

May 12, 2019

Abstract

Joint flexibility is a challenge in industrial robotics that results in unwanted oscillations in the end-effector, unless a specific control law is implemented to prevent this. In recent work, two passivity-based control laws were proposed that address this problem, while at the same time dealing with motor saturation and the absence of adequate velocity measurements.

In this work, these two naturally saturated control laws that only use position measurements are analyzed and tested on a robotic arm with flexible joints, to validate their performance and determine their applicability. The tests consist of two pick and place routines, in which different positions have to be attained in sequence and with a sufficient accuracy. In order to improve the model of the robotic arm, new estimates for the friction parameters were identified, and to create a fully functioning pick and place routine, a suitable controller for the end-effector model was implemented as well.

Results showed that while one controller was not able to eliminate the oscillations without inducing a steady-state error, the second controller successfully deals with both the oscillations and the steady-state error. The structure of this controller gives several opportunities to configure the control parameters to achieve the best performance. Additionally, more insight is given into the structure of the controller by analyzing its performance based on several different configurations of the control parameters.

Contents

Notation

- All vectors are column vectors.
- An $n \times m$ matrix A is denoted by $A_{n\times m}$, an $n \times m$ matrix of zeros by $0_{n\times m}$ and an $n \times n$ identity matrix by $I_{n\times n}$.
- For scalar function $f(x)$ with $x = (x_1, \ldots, x_n)^\top$ the following notation is defined for the partial derivatives

$$\frac{\partial f}{\partial x} := \begin{bmatrix} \frac{\partial f}{\partial x_1} \\ \vdots \\ \frac{\partial f}{\partial x_n} \end{bmatrix}, \qquad \frac{\partial^2 f}{\partial x^2} := \begin{bmatrix} \frac{\partial^2 f}{\partial x_1^2} & \cdots & \frac{\partial^2 f}{\partial x_1 x_n} \\ \vdots & \ddots & \vdots \\ \frac{\partial^2 f}{\partial x_n \partial x_1} & \cdots & \frac{\partial^2 f}{\partial x_n^2} \end{bmatrix}$$

- The use of an asterisk in x_* indicates a constant value, used for the desired position of the robotic arm.
- The following notations indicate that a function $f(x)$ is evaluated at x_*

$$f(x)\Big|_* \iff \Big(f(x)\Big)_* \iff \Big[f(x)\Big]_* \iff f(x_*)$$

- The notation $A = diag\{a_1, a_2\}$ describes a matrix A with diagonal elements a_1 and a_2

$$diag\{a_1, a_2\} = \begin{bmatrix} a_1 & 0 \\ 0 & a_2 \end{bmatrix}$$

- If scalar x can only take positive values, this is denoted by $x \in \mathbb{R}_{>0}$. When it can also take a zero value, this is denoted by $x \in \mathbb{R}_{\geq 0}$.
- The norm of a vector x is denoted by $||x||$

Chapter 1

Introduction

Robotic arms became an essential part of industrial production in the 1970's, when technological advances such as digital computers were developed and their parts became increasingly smaller. This allowed the industrial robots to be programmed and controlled with computers, creating new applications in automating production and manufacturing [17]. An example is the use of a planar robotic arm to move products between conveyor belts and to ensure products are in the desired position for further processing [1]. Initially, the application of robotics was heavily focussed on improving production processes in for instance the automotive industry. Since the 1970's and 1980's, the range of applications of robotics and its body of knowledge has been continually increasing and is used in areas such as biomechanics and surgery, but also in virtual simulations and computer animations [17]. Much progress has been made in the control and analysis of robotic arms, but there remain areas where further improvements can be made. A specific challenge in robotic arms is the phenomenon of joint flexibility, which means that a link in the robotic arm can move slightly independently from the driving actuator, typically manifested by oscillating behavior in the robotic arm.

1.1 Robotic arms with flexible joints

The term joint flexibility is used to describe the phenomenon where the movement of a link in a robotic arm is not exactly equal to the to the movement of the driving actuator, but exhibits elastic behavior. This means that manipulating the angular position and velocity of actuators does not directly result in an equal movement of the links. This phenomenon is common in industrial robots as a result of joint configuration, for instance by using cycloidial gears or harmonic drives [7]. Joint flexibility also arises in other areas, such as service robotics or space robotics, where lightweight robots are developed with a high load to weight ratio [2].

The elastic behavior is manifested by oscillations in the end-effector position, which leads to inaccurate movements and this makes the systems difficult to control and analyse. To counteract this oscillatory behavior at the end-effector, an appropriate control law needs to be implemented [18, 20].

1.2 Recent work

A promising line of research that can facilitate control of nonlinear mechanical systems such as flexible joint robots, is conducted around passivity-based control of port-Hamiltonian systems. The port-Hamiltonian (pH) framework [16] for describing mechanical systems has received a lot of attention in the last two decades, due to its intuitive physical interpretation and useful features in controller design[10, 11, 12, 16]. The structure of pH-systems gives insight into where the energy in the system is either added or dissipated. Another feature of pH-systems is that they are passive, which means that they cannot generate energy by themselves. This passivity feature allows for a specific category of control methods to be used: passivity-based control (PBC).

In recent work [4, 19], passivity-based control laws were designed and tested in a setpoint regulation for a flexible joint planar robotic arm. These controllers performed significantly better than an LQR controller they were compared with. One major drawback of the presented controllers in [19] is the lack of accuracy; a steady state error was often still present in the experimental results. Moreover, the proposed controllers were only tested on a single setpoint regulation, which leaves some room to investigate their performance on more challenging tasks.

In this work, the research on the analysis and control of a planar robotic arm with rotational flexible joints will be continued. The applicability of passivity-based control laws in industrial settings will be investigated further, by experimenting with their implementation in pick and place routines.

Pick and place routines are common in industrial production and manufacturing, and testing the control laws on a pick and place routine creates more insight in possible issues that can not be revealed in regular setpoint regulations. Pick and place routines require precise and smooth movements of various displacements.

1.3 Research goal

Flexibility in the joints impairs the accurate movements of a robotic arm, so specific controllers that are capable to effectively counteract the unwanted consequences of joint flexibility must be designed. In this work, recently proposed control laws are tested to determine whether they enable an accurate and smooth movement in a planar robotic arm with two flexible joints, such that a pick and place routine can be performed.

To create a stronger connection to practical implementation, two other common issues concerning the limitations in sensors and actuators are taken into account.

Firstly, actuators have maximum currents that are imposed to keep the system within safe limits of operation. If the input signal for an actuator is too large, the equipment can be irreversibly damaged, which means that the input signal for an actuator must be saturated. If the actuator saturation is not taken into account in the control design, this can have a negative effect on the system's performance. This happens because the input signal to the motor is cut off when it becomes too

large. Thus, the controller is expected to have a larger impact on the system than it actually has, which means the actual performance is worse than expected. For these reasons, it is interesting to research control laws that are naturally saturated, which means that they can be configured such that the input signal to the motor never exceeds a pre-specified limit.

The second issue that will be taken into account is the lack of accurate velocity measurements. Information on the velocity in a mechanical system is useful in control design, which can be used to increase the controller performance, for instance in PID control. Unfortunately, the estimates for the velocity can be unreliable. Information on the velocity is obtained by implementing a derivative filter on the position measurements, but the noise and measurement errors are amplified in the differentiation, which has a negative effect on the system's performance. For these reasons, it is beneficial to for a control law to only use positional measurements.

The main research goal is to find a naturally saturated control law, which only uses position measurements, and that can accomplish a high-precision pick and place routine for a planar robotic arm with flexible joints. Two important performance indicators of the control law will be the absence of oscillations and the time in which the steady state can be reached.

1.4 Outline of the document

In the Chapter 2, the mathematical background that is needed for the system description and controller design is presented and explained. Afterwards, the mathematical model of the system in both the rigid and the flexible setup is given in Chapter 3. In Chapter 4, the control laws that are used in the experiments are presented and proofs are given for stability. Then, the experimental setup for the pick and place routines is explained in Chapter 5. The results of testing control laws these control laws in the proposed experiments are discussed in the Chapter 6, followed by Chapter 7 where the findings in this work are discussed in a broader sense, taking into account the context of practical challenges and future research.

Chapter 2

Preliminaries

In this chapter, the theoretical background is provided which is required to understand the model description, control design and results. The nonlinear systems in this research are described in the port-Hamiltonian framework. Important notions regarding the control of these systems are Lyapunov's stability theory and passivity theory. Lastly, the fundamentals from the passivity-based control methodology are presented, which forms the basis of the used controllers.

2.1 Stability of nonlinear systems

All physical systems, mathematical equations, and natural phenomena can be categorized as either linear or nonlinear. All linear systems satisfy a common principle of *superposition*, which is used in practically all methods that solve or analyze linear problems. Unfortunately, the superposition principle does not apply to nonlinear systems, so the useful methods that can be used on linear systems cannot be applied here [3, 6].

Due to their diversity and complex behavior, there is not one framework or methodology with which all nonlinear systems can be analyzed. However, there are tools that can be used to analyze specific types of nonlinear systems. One of these tool is Lyapunov's stability theory, which will be explained in this section.

Stability is an important concept in control theory and engineering that is related to how a system behaves. For mechanical systems such as the one that is the subject of this thesis, we often want the system to converge towards a certain equilibrium point, and to analyze this type of stability, Lyapunov's theory is typically used. First, several stability concepts will be defined, and then Lyapunov's direct method for analysing stability in nonlinear systems will be explained. A more extensive review of the information that is given in this section, along with the proofs for the theorems can be found in the book *Nonlinear systems*, by Hassan Khalil [13].

Consider the autonomous system

$$\dot{x} = f(x), \tag{2.1}$$

where $f : \mathcal{D} \to \mathbb{R}^n$ is a locally Lipschitz map from a domain $\mathcal{D} \subset \mathbb{R}^n$ into $\mathbb{R}^n$. Suppose that x^* is an equilibrium point of (2.1), $f(x^*) = 0$. We can assume that $x^* = 0$ without loss of generality, because any point can be shifted to the origin via a change of variables.

Definition 2.1.1. Stability in the sense of Lyapunov
The equilibrium point $x^* = 0$ of (2.1) is called

Stable if for all $\epsilon > 0$ there exists a $\delta = \delta(\epsilon) > 0$ such that

$$||x(0)|| < \delta \Rightarrow ||x(t)|| < \epsilon, \quad \forall t \geq 0$$

Unstable if it is not stable

Asymptotically stable if it is stable and if δ can be chosen such that

$$||x(0)|| < \delta \Rightarrow \lim_{t \to \infty} x(t) = 0$$

In other words, a system is stable when each solution that starts close to the equilibrium point remains close to it, while for asymptotic stability each solution close to the equilibrium point converges to the equilibrium when time goes to infinity.

Lyapunov's second method, also known as Lyapunov's direct method, will form a strong basis of the controllers that are to be designed.

Theorem 2.1.1. ***Lyapunov's direct method***
Let $x = 0$ be an equilibrium point for (2.1) and $D \subset \mathbb{R}^n$ be a domain containing $x = 0$. Let $\mathcal{V} : \mathcal{D} \to \mathbb{R}$ be a continuously differentiable function, such that

$$\begin{aligned} &\mathcal{V}(0) = 0 \\ &\mathcal{V}(x) > 0, \quad \forall x \neq 0 \\ &\dot{\mathcal{V}}(x) \leq 0, \quad \forall x \in \mathcal{D} \end{aligned} \tag{2.2}$$

then $x = 0$ is stable. Moreover, if

$$\dot{\mathcal{V}}(x) < 0, \quad \forall x \neq 0 \tag{2.3}$$

then $x = 0$ is asymptotically stable. ◁

A function $\mathcal{V}$ is a Lyapunov function if it satisfies the three equations in (2.2). Moreover, if the inequality (2.3) can be proven, that the equilibrium point is asymptotically stable. Additionally, if $\mathcal{V}$ is *radially unbounded*, then the equilibrium point is globally asymptotically stable.

Definition 2.1.2. Radially unboundedness
A function $\mathcal{V}(x)$ is called radially unbounded when

$$||x|| \to \infty \quad \Rightarrow \quad \mathcal{V}(x) \to \infty \tag{2.4}$$

However, it often happens that the equilibrium point is not asymptotically stable, because $\dot{\mathcal{V}}$ is only negative semi-definite and thus does not satisfy (2.3). This happens for instance when $\dot{\mathcal{V}}$ does not depend on all states. In this case, asymptotic stability can still be proven using the Barbashin theorem.

Theorem 2.1.2. ***Barbashin***
Let $x = 0$ be an equilibrium point for (2.1). Let $V : D \to R$ be a continuously differentiable positive definite function on a domain D containing the origin $x = 0$, such that $\dot{V}(x) \leq 0$ in D. Let $S = \{x \in D \mid \dot{V}(x) = 0\}$ and suppose that no solution can stay identically in S, other than the trivial solution $x(t) \equiv 0$. Then the origin is asymptotically stable. ◁

For more information on Barbashin's theorem, the reader is referred to Corollary 4.1 from [13].

When the stability of a system cannot be determined using Lyapunov's direct method, another possibility is to use *Lyapunov's indirect method*. This method uses a linearization of the nonlinear system around its equilibrium point, and determines its stability based on the eigenvalues of the closed-loop system matrix. The stability of the linearized system means that the nonlinear system is locally stable.

Theorem 2.1.3. ***Lyapunov's indirect method***
Consider again the autonomous system (2.1) with equilibrium point $x_* = 0$, and define

$$A = \left.\frac{\partial f(x)}{\partial x}\right|_* \tag{2.5}$$

If the real parts of the eigenvalues of A are all negative, then the equilibrium point x_* is asymptotically stable. The asymptotic stability of the linearized systems determine the local asymptotic stability of the nonlinear system. ◁

Additionally, the matrix A is called *Hurwitz* if the real parts of its eigenvalues are all negative.

2.2 Passivity theory

Passivity is a property of many physical systems and is closely related to the dissipation and transformation of energy. Passive systems are systems that cannot store more energy than is supplied to it, which means that there is no internal creation of energy [16, 21]. The difference between the energy that is supplied to the system and the energy that is stored in the system is the dissipated energy. In the concept of passivity, the energy storage is based on the relation between inputs and outputs in a system and is in this sense also connected to the stability

of the system [16]: a system is stable when a bounded energy input results in a bounded energy output [13].

Consider a general state-space system of the form:

$$\begin{aligned} \dot{x} &= f(x,u) \\ y &= h(x,u) \end{aligned} \tag{2.6}$$

Where input $u \in \mathbb{R}^m$, output $y \in \mathbb{R}^p$ and $x \in \mathbb{R}^n$, and consider a function $s(u(t), y(t)) = u^\top(t)y(t)$, called the *supply rate*.

Definition 2.2.1. Passivity
A system of the form (2.6) is *passive*, if there exists a *storage function* $S\colon \mathbb{R}^n \to \mathbb{R}^+$, such that for all $x_0 \in \mathbb{R}^n$, all $t_1 \geq t_0$, and all input functions $u(\cdot)$

$$S(x(t_1)) \leq S(x(t_0)) + \int_{t_0}^{t_1} u^\top(t)y(t)dt, \tag{2.7}$$

where $x(t_0) = x_0$, and $x(t_1)$ is the state of (2.6) at time t_1 resulting from initial condition x_0 and input function $u(\cdot)$. Here, $y(t)$ is called the *passive output* of the system.

The inequality (2.7) expresses that the stored energy at any future time t_1 can never be greater than the stored energy at t_0 and the supplied energy during time interval $[t_0, t_1]$. By definition, there can be no internal creation of energy, only internal dissipation of energy is possible. Note that the inequality sign stems from the fact that the dissipated energy is extracted from the system. If (2.7) holds with *equality* for all x_0 and all $u(\cdot)$, then the system (2.6) is called *lossless*.

Alternatively, equation (2.7) can also be rewritten as a power inequality

$$\dot{S}(x(t)) \leq u^\top(t)y(t), \tag{2.8}$$

showing that the time-derivative of the storage function must be smaller than or equal to the supply rate.

For a more thorough description of passivity and passive systems, the reader is referred to [16].

2.3 Port-Hamiltonian framework for mechanical systems

Robotic arms are physical, mechanical systems whose dynamics can be described in the port-Hamiltonian (pH) framework. The pH-framework has been proven useful in controlling mechanical systems, and it has gained a lot of attention in the last two decades [10, 11, 12, 16]. It combines the Hamiltonian equations of motion with concepts from port-based network modeling, such as energy dissipation and power-conserving interconnection [16]. The Hamiltonian function that forms the

basis of the dynamics is a function that naturally satisfies the dissipation inequality (2.7), since it is defined as the total energy in the system. As a consequence of the definition of pH-systems, they have an intuitive physical interpretation and they are passive by design, which is a useful feature that can be exploited in analysis and control design.

The dynamics of a pH-system are defined by the Hamiltonian equations of motion

$$\begin{aligned} \dot{q} &= \frac{\partial H}{\partial p}(q,p) \\ \dot{p} &= -\frac{\partial H}{\partial q}(q,p) + \tau \end{aligned} \tag{2.9}$$

where $q = col(q_1, \ldots, q_r)$ are the generalized displacement coordinates, and $p = col(p_1, \ldots, p_r)$ the corresponding generalized momenta in a system with r degrees of freedom.

Additionally, the Hamiltonian function $H(q,p) = T + V$ is the total energy in the system, consisting of the *kinetic* energy T and the *potential* energy V, and τ represents the external forces acting on the system.

To determine the correct Hamiltonian for a system, the kinetic and potential energies must be defined. While potential energy can take different forms (e.g. gravitational or elastic) in mechanical systems, the kinetic energy is usually of the following form:

$$T(q,\dot{q}) = \frac{1}{2}\dot{q}^\top M(q)\dot{q}, \tag{2.10}$$

where $M(q)$ is the generalized mass-inertia matrix, which is symmetric and positive definite for all q. Using the definition of momenta $p = M(q)\dot{q}$, the kinetic energy can be rewritten into

$$T(q,p) = \frac{1}{2}p^\top M^{-1}(q)p, \tag{2.11}$$

Now, the Hamiltonian can be written as:

$$H(q,p) = \frac{1}{2}p^\top M^{-1}(q)p + V(q) \tag{2.12}$$

When we take the Hamiltonian as a storage function, it becomes clear that the system with input τ is passive with respect to the passive output $\dot{q}$:

$$\begin{aligned} \dot{H}(q,p) &= (\frac{\partial H}{\partial q})^\top \dot{q} + (\frac{\partial H}{\partial p})^\top \dot{p} \\ &= (\frac{\partial H}{\partial q})^\top \frac{\partial H}{\partial p} - (\frac{\partial H}{\partial p})^\top (\frac{\partial H}{\partial q} - \tau) \\ &= (\frac{\partial H}{\partial p})^\top \tau \\ &= \dot{q}^\top \tau \end{aligned} \tag{2.13}$$

Comparing (2.13) to the power imbalance (2.8) from the previous section, we can conclude that the pH-system is in fact lossless.

The Hamiltonian equations of motion given in (2.9) can be adjusted to include damping matrix $R \in \mathbb{R}^{n\times n}$. To given more insight in the structure of the system, it is written in matrix form:

$$\begin{aligned} \begin{bmatrix} \dot{q} \\ \dot{p} \end{bmatrix} &= \begin{bmatrix} 0_{n\times n} & I_{n\times n} \\ -I_{n\times n} & -R_{n\times n} \end{bmatrix} \begin{bmatrix} \frac{\partial H}{\partial q}(q,p) \\ \frac{\partial H}{\partial p}(q,p) \end{bmatrix} + \begin{bmatrix} 0_{n\times m} \\ B(q)_{n\times m} \end{bmatrix} u \\ y &= B^\top(q)\frac{\partial H}{\partial p}(q,p) \\ q, p &\in \mathbb{R}^n, \quad u \in \mathbb{R}^m \end{aligned} \tag{2.14}$$

Note that, when m equals n, the system is fully actuated, and when $m < n$ the systems is underactuated.

The pH-system model can be generalized further to allow for generalized state variables $x = (x_1, \ldots, x_{2n})^\top$. Then, the system is expressed as

$$\begin{aligned} \dot{x} &= \big(J(x) - \mathcal{R}(x)\big)\frac{\partial H}{\partial x}(x) + g(x)u, \qquad x \in \mathbb{R}^{2n} \\ y &= g^\top(x)\frac{\partial H}{\partial x}(x), \qquad y \in \mathbb{R}^m \end{aligned} \tag{2.15}$$

where matrices $J(x), \mathcal{R}(x) \in \mathbb{R}^{2n\times 2n}$ are called the *interconnection matrix* and the *damping matrix* respectively. $J(x)$ must be skew-symmetric and $\mathcal{R}(x)$ must be symmetric and positive semi-definite, mathematically expressed as

$$\begin{aligned} J(x) &= -J(x)^\top \\ \mathcal{R}(x) &= \mathcal{R}(x)^\top \geq 0 \end{aligned} \tag{2.16}$$

Comparing (2.14) and (2.15), it should be noted that

$$\begin{bmatrix} 0_{n\times n} & I_{n\times n} \\ -I_{n\times n} & -R_{n\times n} \end{bmatrix} = \big(J(x) - \mathcal{R}(x)\big) \tag{2.17}$$

For more information regarding pH-systems, the reader is referred to [16].

2.4 Passivity-based control of pH-systems

The passivity property of PH systems which was shown in the previous section can be used in controller design, a method known known as passivity-based control (PBC). The concept behind this method is that the input can be designed to ensure the system is passive, while placing the minimum of the storage function at the desired equilibrium, ensuring stability at the equilibrium point. The main PBC method that is used in this thesis is based in [4], where a constructive procedure is used to shape the energy without the need for solving partial differential equations.

Recall the general PH-system described by (2.9). PBC aims to find a feedback control law

$$u = a(x) + v \tag{2.18}$$

that transforms the original PH-system with Hamiltonian storage function $H(x)$ into a new PH-system with desired Hamiltonian $H_d(x)$, which has its minimum at the desired equilibrium point x^*.

$$\begin{aligned} \dot{x} &= \big(J(x) - R(x)\big)\frac{\partial H_d}{\partial x}(x) + g(x)u, \qquad y \in \mathbb{R}^m \\ y &= g^\top(x)\frac{\partial H_d}{\partial x}(x), \qquad y \in \mathbb{R}^m \end{aligned} \tag{2.19}$$

The time-derivative of this desired Hamiltonian becomes:

$$\dot{H}_d = -\Big(\frac{\partial H_d}{\partial x}(x)\Big)^\top R(x)\frac{\partial H_d}{\partial x}(x) + y^\top v \tag{2.20}$$

An appropriate function for v can be designed to render the system asymptotically stable.

Now that the mathematical background for this work is presented and explained, the next part presents the mathematical model of the robotic arm that will be used for the experiments and simulations. Afterwards, the controller designs are discussed and the results are presented.

Chapter 3

Model Description

The robotic arm that will be used throughout this research is a Quanser 2 DOF Serial Flexible Joint. This is a planar robotic arm with two joints, that can be configured to either be flexible or rigid. The two joints of this robotic arm are each actuated by one motor, and sensors are placed at each joint to measure the angular displacement of both the motor and the link. Flexibility in the joints is achieved by connecting the link and the motor in both joints with two springs. In the rigid configuration, these springs are made redundant by attaching a rigid bar that connects both ends of the spring.

The experimental setup of this arm that is available at the University of Groningen (shown in figure 3.1) has an additional end-effector attached to it, with which small items can be gripped and moved. The end-effector does not exhibit flexibility, and functions only to perform the pick and place task.

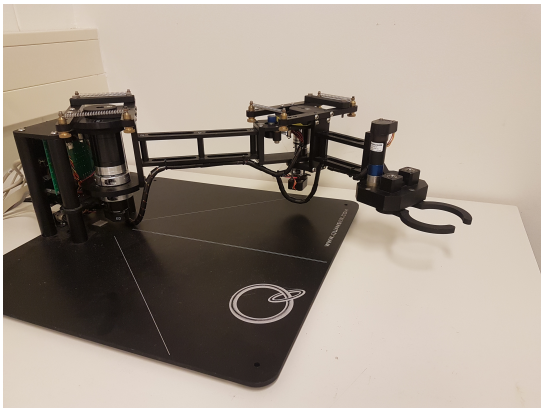

Figure 3.1: The Quanser 2 DOF Serial Flexible Joint with end-effector.

In following section, the complete mathematical model of the system in the flexible configuration will be described as a pH-system. Then, the model of the rigid configuration is given, which is a simplification of the flexible model, with fewer state variables and a simplified energy function.

3.1 Flexible Model

To mathematically describe the system in the pH-form, first the state variables need to be defined. We define the angular position of the i-th link by q_{l_i}, and the angular position of the i-th motor by q_{m_i}. Let $q = [q_l, q_m]^\top$ be the (angular) position vector of links and motors, and let $p = [p_l, p_m]^\top$ be the corresponding momenta. Thus, for the robotic arm with 2 links we have

$$q = \begin{bmatrix} q_l \\ q_m \end{bmatrix} = \begin{bmatrix} q_{l_1} \\ q_{l_2} \\ q_{m_1} \\ q_{m_2} \end{bmatrix}, \quad p = \begin{bmatrix} p_l \\ p_m \end{bmatrix} = \begin{bmatrix} p_{l_1} \\ p_{l_2} \\ p_{m_1} \\ p_{m_2} \end{bmatrix} \tag{3.1}$$

The corresponding dynamics are expressed as

$$\begin{bmatrix} \dot{q} \\ \dot{p} \end{bmatrix} = \begin{bmatrix} 0_{4\times4} & I_{4\times4} \\ -I_{4\times4} & -R_{4\times4} \end{bmatrix} \begin{bmatrix} \frac{\partial H}{\partial q}(q,p) \\ \frac{\partial H}{\partial p}(q,p) \end{bmatrix} + \begin{bmatrix} 0_{4\times2} \\ B \end{bmatrix} u, \quad u \in \mathbb{R}^2 \tag{3.2}$$

with

$$\begin{aligned} R_{4\times4} = \begin{bmatrix} D_l & 0_{2\times2} \\ 0_{2\times2} & D_m \end{bmatrix}, \quad B = \begin{bmatrix} 0_{2\times2} \\ I_{2\times2} \end{bmatrix} \\ D_l = diag\{D_{l_1}, D_{l_2}\}, \quad D_m = diag\{D_{m_1}, D_{m_2}\} \end{aligned} \tag{3.3}$$

Since $q, p \in \mathbb{R}^4$ and $u \in \mathbb{R}^2$, the system is under-actuated.

To derive the Hamiltonian function, the kinetic energy and the potential energy in the system are determined, recall (2.12).

Kinetic energy is present in both the links and the motors as a result of their movement. Following the general form of kinetic energy, we have

$$\begin{aligned} T_l(q_l, p_l) &= \frac{1}{2} p_l^\top M_l^{-1}(q_{l_2}) p_l, \\ T_m(q_m, p_m) &= \frac{1}{2} p_m^\top M_m^{-1} p_m \end{aligned}$$

Here, $M_l(q_l), M_m(q_m) \in \mathbb{R}^{2x2}$ are the inertia matrices, which are symmetric and positive definite.

Potential energy in the system only consists of the energy in the springs. Gravitational energy is ignored because the robotic arm is only active in the horizontal plane. Potential energy in a spring is of the form $\frac{1}{2}kx^2$, where k is the spring constant and x is the displacement. For the springs in the robotic arm we have

$$V(q_l, q_m) = \frac{1}{2}(q_l - q_m)^\top K_s (q_l - q_m)$$

Here, $K_s \in \mathbb{R}^{2x2}$ is the symmetric and positive definite spring matrix.

Now we can construct the Hamiltonian as follows:

$$\begin{aligned} H(q,p) &= T_l + T_m + V \\ &= \frac{1}{2} p_l^\top M_l^{-1}(q_{l_2}) p_l + \frac{1}{2} p_m^\top M_m^{-1} p_m + \frac{1}{2}(q_l - q_m)^\top K_s (q_l - q_m) \\ &= \frac{1}{2} p^\top M(q)^{-1} p + \frac{1}{2}(q_l - q_m)^\top K_s (q_l - q_m) \end{aligned}$$

Here, the p_l and p_m vectors are stacked as in (3.1) and we define

$$M(q_{l_1}) = \begin{bmatrix} M_l(q_{l_2}) & 0 \\ 0 & M_m \end{bmatrix}$$

To define the mass-inertia matrices we need the link length l_i, link mass m_i, distance to center of mass of the link r_i, moment of inertia for the links I_{l_i} and for the motors I_{m_i}.

As in [8], the mass-inertia matrix for the links is defined using the constants

$$\begin{aligned} a_1 &= m_1 r_1^2 + m_2 l_1^2 + I_{l_1} \\ a_2 &= m_2 r_2^2 + I_{l_2} \\ b &= m_2 l_1 r_2 \end{aligned}$$

The mass-inertia matrices $M_l(q_{l_2})$ and M_m are defined as

$$M_l(q_{l_2}) = \begin{bmatrix} a_1 + a_2 + 2b\cos q_{l_2} & a_2 + b\cos q_{l_2} \\ a_2 + b\cos q_{l_2} & a_2 \end{bmatrix}, \qquad M_m = \begin{bmatrix} I_{m_1} & 0 \\ 0 & I_{m_2} \end{bmatrix}$$

It should be noted at this point that the mass-inertia matrix for the motors is a constant, while the mass-inertia matrix for the links depends on the angular position of the second link, q_{l_2}. The values for the parameters that are used in the model are given in table 3.1. Here D_l and D_m represent the damping in the links and in the motors respectively, and A_{max} is the maximum current through the motor at each link. The values for D_l, D_m and I_m are taken from [14], and the remaining parameters can be found in the reference manual for the Quanser 2-DOF Serial Flexible Joint Robot. have been determined experimentally, More information regarding the calculations for D_l and D_m can be found in Appendix A.

parameter	joint 1	joint 2	unit
l	0.343	0.267	$[m]$
m	0.5	1	$[kg]$
r	0.2	0.25	$[m]$
I_l	0.01	0.01	$[kg \cdot m^2]$
I_m	0.217	0.007	$[kg \cdot m^2]$
K_s	9	4	$[N \cdot m/rad]$
D_l	0.038	0.03	$[N \cdot m \cdot s/rad]$
D_m	8.435	0.136	$[N \cdot m \cdot s/rad]$
A_{max}	0.944	1.21	$[A]$

Table 3.1: Model parameters for the Quanser 2 DOF Serial Flexible Joint

3.2 Rigid Model

In the rigid configuration, the link angles always equals the motor angles, thus there is no need to define a state for both. The position and momenta vectors become:

$$q = \begin{bmatrix} q_1 \\ q_2 \end{bmatrix} \quad p = \begin{bmatrix} p_1 \\ p_2 \end{bmatrix} \tag{3.4}$$

And the dynamics of the systems are expressed as:

$$\begin{bmatrix} \dot{q} \\ \dot{p} \end{bmatrix} = \begin{bmatrix} 0_{2\times2} & I_{2\times2} \\ -I_{2\times2} & R_{2\times2} \end{bmatrix} \begin{bmatrix} \frac{\partial H}{\partial q}(q,p) \\ \frac{\partial H}{\partial p}(q,p) \end{bmatrix} + \begin{bmatrix} 0_{2\times2} \\ B \end{bmatrix} u \tag{3.5}$$

In this case the system is fully actuated, since $q, p \in \mathbb{R}^2$ and $u \in \mathbb{R}^2$ as well. Additionally, the springs have no effect in the rigid configuration, so there is no potential energy in the systems which simplifies the Hamiltonian to the following

$$H(q,p) = \frac{1}{2} p^\top M(q)^{-1} p \tag{3.6}$$

where $M = M_l + M_m$.

This concludes the pH-system model for the flexible and the rigid configuration. The models that are presented here are used in analysis and in the simulations. In the next section, the end-effector will be briefly discussed.

3.3 End-effector

Because the end-effector of the robotic arm was custom made and it has never been used before, there is no available model that can be used.

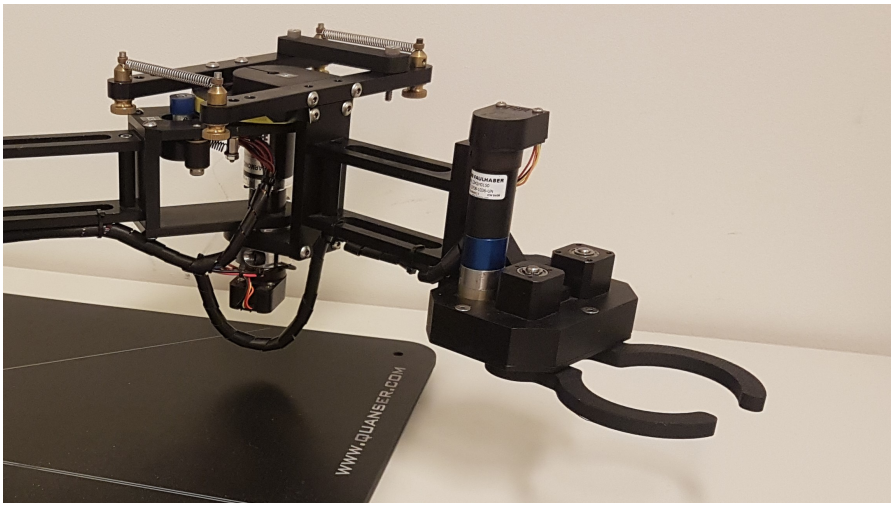

Figure 3.2: The second joint and second link with the end-effector attached.

The end-effector consists of two arms, which are coupled such that their movements are indentical. Small objects can be gripped by closing these arms together. The end-effector is actuated by a DC-motor that can open and close the arms of the end-effector.

The maximum rotation of the arms in the end-effector is approximately 185°, or 3.23 [rad], between fully opened and fully closed. This range of angular displacement corresponds with 87102 steps in the encoder, and there is a linear relation between the end-effector angle and the encoder steps. Thus, number of encoder steps per degree is 470.8.

An important note is that the encoding is relative, which means that the absolute position can not be read, and the initial position at the beginning of an experiment is taken to be 0.

Unfortunately, there was no information available on the specific system parameters, which limits the possibilities of building an accurate model. Further identification of the dynamics of end-effector falls outside of the scope of this research. A linear model is assumed, friction is not taken into account and the end-effector will be controlled with a PI-controller.

Chapter 4

Controller design

In this chapter, the control laws will be designed that will be tested in the pick and place routine experiments. First, a controller is presented that is naturally saturated and which only uses position measurements. The second controller is an adaptation on the first one, adding an extra element to improve the performance. In the final section of this chapter, the control of the end-effector is discussed.

4.1 Saturated control without velocity measurements

In [5], a naturally saturated control law is proposed that only uses position measurements. Damping is injected into the closed-loop system by means of a virtual state that is linearly related to the positions, a method that was proposed in [9].

To apply this method, the definitions of two new variables is needed

$$\begin{aligned} z_l(q_l, x_{c_l}) &:= q_l - q_* + x_{c_l} \\ z_m(q_m, x_{c_m}) &:= q_m - q_* + x_{c_m} \end{aligned} \tag{4.1}$$

In this equation x_{c_l} and x_{c_m} are the virtual states that are used to inject damping. In Proposition 4.1.1, the control law is presented.

Proposition 4.1.1. *First, define the functions*

$$\begin{aligned} \phi_l(z_l) &:= \sum_{i=1}^{2} \frac{\alpha_{l_i}}{\beta_{l_i}} \ln\left(\cosh\left(\beta_{l_i} z_{l_i}\right)\right) \\ \phi_m(z_m) &:= \sum_{i=1}^{2} \frac{\alpha_{m_i}}{\beta_{m_i}} \ln\left(\cosh\left(\beta_{m_i} z_{m_i}\right)\right) \end{aligned} \tag{4.2}$$

where $\alpha_{l_i}, \alpha_{m_i}, \beta_{l_i}, \beta_{m_i} \in \mathbb{R}_{\geq 0}$. *Consider the dynamics*

$$\begin{aligned} \dot{x}_{c_l} &= -R_{c_l} \frac{\partial \phi_l}{\partial x_{c_l}}(z_l(q_l, x_{c_l})) \\ \dot{x}_{c_m} &= -R_{c_m} \left(\frac{\partial \phi_m}{\partial x_{c_m}}(z_m(q_m, x_{c_m})) + K_c x_{c_m} \right) \end{aligned} \tag{4.3}$$

where $R_{c_l}, R_{c_m}, K_c \in \mathbb{R}^{2\times 2}$ *are positive definite constant matrices verifying*

$$R_{c_l} - \frac{1}{4}(D_l^{-1} + D_m^{-1}) > 0. \tag{4.4}$$

Finally, consider the control law

$$u = -\frac{\partial \phi_l}{\partial z_l}(z_l(q_l, x_{c_l})) - \frac{\partial \phi_m}{\partial z_m}(z_m(q_m, x_{c_m})). \tag{4.5}$$

Then:

1. *The control signal* u *given in* (4.5) *is naturally saturated with configurable saturation limits.*

2. *Consider the dynamics of the augmented state space* $\zeta = \left[q^\top, p^\top, x_{c_l}^\top, x_{c_m}^\top\right]^\top$, *given by* (3.2) *and* (4.3). *This system in closed-loop with control law* (4.5) *admits a pH representation.*

3. *The solution* $\zeta_* := (q_l, q_m, p_l, p_m, x_{c_l}, x_{c_m}) = (q_*, q_*, 0_2, 0_2, 0_2, 0_2)$ *is an globally asymptotically stable equilibrium point of the closed-loop system with Lyapunov function*

$$H_\zeta(\zeta) = H(q,p) + \phi_l(z_l(q_l, x_{c_l})) + \phi_m(z_m(q_m, x_{c_m})) + \frac{1}{2} x_{c_m}^\top K_c x_{c_m} \tag{4.6}$$

Proof. Firstly, it is straightforward to show that the elements of control signal u is saturated, when it is noted that

$$\begin{aligned} \frac{\partial \phi_l}{\partial z_l}(z_l(q_l, x_{c_l})) &= \begin{bmatrix} \alpha_{l_1} \tanh(\beta_{l_1} z_{l_1}) \\ \alpha_{l_2} \tanh(\beta_{l_2} z_{l_2}) \end{bmatrix} \\ \frac{\partial \phi_m}{\partial z_m}(z_m(q_m, x_{c_m})) &= \begin{bmatrix} \alpha_{m_1} \tanh(\beta_{m_1} z_{m_1}) \\ \alpha_{m_2} \tanh(\beta_{m_2} z_{m_2}) \end{bmatrix} \end{aligned}. \tag{4.7}$$

This reduces the control law (4.5) to

$$\begin{bmatrix} u_1 \\ u_2 \end{bmatrix} = \begin{bmatrix} -\alpha_{l_1} \tanh(\beta_{l_1} z_{l_1}) - \alpha_{m_1} \tanh(\beta_{m_1} z_{m_1}) \\ -\alpha_{l_2} \tanh(\beta_{l_2} z_{l_2}) - \alpha_{m_2} \tanh(\beta_{m_2} z_{m_2}) \end{bmatrix}. \tag{4.8}$$

Due to the form of the hyperbolic tangent, as shown in figure 4.1, this means that

$$-(\alpha_{l_i} + \alpha_{m_i}) \leq u_i \leq \alpha_{l_i} + \alpha_{m_i} \tag{4.9}$$

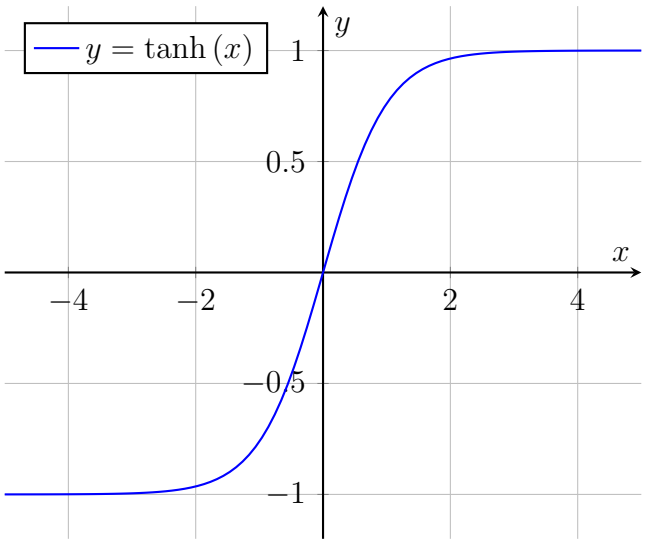

Figure 4.1: Plot of the $\tanh(x)$ function

hence, the elements of the control signal u are saturated.

Secondly, to proof that the system (3.2) in closed-loop with (4.5) admits a pH representation when the augmented state space $\zeta = \left[q^\top, p^\top, x_{c_l}^\top, x_{c_m}^\top\right]^\top$ is used, the dynamics of all states must first be described in terms of the new Hamiltonian function H_ζ [1].

$$\begin{aligned} H_\zeta &= H + \phi_l + \phi_m + \frac{1}{2} x_{c_m}^\top K_c x_{c_m} \\ \text{with} \quad H &= \frac{1}{2} p^\top M^{-1} p + \frac{1}{2}(q_l - q_m)^\top K_s (q_l - q_m) \end{aligned} \tag{4.10}$$

We can see directly that for the states q we have

$$\dot{q} = \frac{\partial H}{\partial p} = \frac{\partial H_\zeta}{\partial p} \tag{4.11}$$

Recall (4.1) and note that

$$\frac{\partial z_l}{\partial q_l} = \frac{\partial z_l}{\partial x_{c_l}} = \frac{\partial z_m}{\partial q_m} = \frac{\partial z_m}{\partial x_{c_m}} = I_{2\times 2}. \tag{4.12}$$

Using the chain rule, it can also be deduced that

$$\frac{\partial \phi_l}{\partial q_l} = \frac{\partial \phi_l}{\partial x_{c_l}} = \frac{\partial \phi_l}{\partial z_l} = \frac{\partial H_\zeta}{\partial x_{c_l}}, \quad \text{and} \quad \frac{\partial \phi_m}{\partial q_m} = \frac{\partial \phi_m}{\partial x_{c_m}} = \frac{\partial \phi_m}{\partial z_m} \tag{4.13}$$

The dynamics of the momenta of the links and the motors will now be described in terms of H_ζ. First recall

$$\dot{p}_l = -\frac{\partial H}{\partial q_l} - D_l \frac{\partial H}{\partial p_l} \tag{4.14}$$

[1] For readability, the arguments will be left out in the following equations.

and note that

$$\frac{\partial H}{\partial q_l} = \frac{\partial H_\zeta}{\partial q_l} - \frac{\partial \phi_l}{\partial q_l} = \frac{\partial H_\zeta}{\partial q_l} - \frac{\partial H_\zeta}{\partial x_{c_l}}, \quad \text{and} \quad D_l \frac{\partial H}{\partial p_l} = D_l \frac{\partial H_\zeta}{\partial p_l} \tag{4.15}$$

Thus,

$$\dot{p}_l = -\frac{\partial H_\zeta}{\partial q_l} + \frac{\partial H_\zeta}{\partial x_{c_l}} - D_l \frac{\partial H_\zeta}{\partial p_l} \tag{4.16}$$

In a similar fashion we recall

$$\dot{p}_m = -\frac{\partial H}{\partial q_m} - D_m \frac{\partial H}{\partial p_m} + u \tag{4.17}$$

and observe that

$$\frac{\partial H}{\partial q_m} = \frac{\partial H_\zeta}{\partial q_m} - \frac{\partial \phi_m}{\partial q_m}, \quad \text{and} \quad D_m \frac{\partial H}{\partial p_m} = D_m \frac{\partial H_\zeta}{\partial p_m} \tag{4.18}$$

Thus, when we insert control law (4.5) into (4.17), and apply (4.13) and (4.18), we obtain,

$$\begin{aligned}
\dot{p}_m &= -\frac{\partial H}{\partial q_m} - D_m \frac{\partial H}{\partial p_m} - \frac{\partial \phi_l}{\partial z_l} - \frac{\partial \phi_m}{\partial z_m} \\
\dot{p}_m &= -\frac{\partial H_\zeta}{\partial q_m} + \frac{\partial \phi_m}{\partial q_m} - D_m \frac{\partial H_\zeta}{\partial p_m} - \frac{\partial \phi_l}{\partial z_l} - \frac{\partial \phi_m}{\partial z_m} \\
\dot{p}_m &= -\frac{\partial H_\zeta}{\partial q_m} - Dm \frac{\partial H_\zeta}{\partial p_m} - \frac{\partial H_\zeta}{\partial x_{c_l}}
\end{aligned} \tag{4.19}$$

Now, for the two virtual states x_{c_l} and x_{c_m}, the dynamics from (4.3) can be rewritten into

$$\dot{x}_{c_l} = -R_{c_l} \frac{\partial H_\zeta}{\partial x_{c_l}}, \quad \text{and} \quad \dot{x}_{c_m} = -R_{c_m} \frac{\partial H_\zeta}{\partial x_{c_m}} \tag{4.20}$$

Hence, from (4.11), (4.16), (4.19) (4.20), the closed-loop system takes the form of

$$\begin{bmatrix} \dot{q}_l \\ \dot{q}_m \\ \dot{p}_l \\ \dot{p}_m \\ \dot{x}_{c_l} \\ \dot{x}_{c_m} \end{bmatrix} = \begin{bmatrix} 0_{2\times2} & 0_{2\times2} & I_{2\times2} & 0_{2\times2} & 0_{2\times2} & 0_{2\times2} \\ 0_{2\times2} & 0_{2\times2} & 0_{2\times2} & I_{2\times2} & 0_{2\times2} & 0_{2\times2} \\ -I_{2\times2} & 0_{2\times2} & -D_l & 0_{2\times2} & I_{2\times2} & 0_{2\times2} \\ 0_{2\times2} & -I_{2\times2} & 0_{2\times2} & -D_m & -I_{2\times2} & 0_{2\times2} \\ 0_{2\times2} & 0_{2\times2} & 0_{2\times2} & 0_{2\times2} & -R_{c_l} & 0_{2\times2} \\ 0_{2\times2} & 0_{2\times2} & 0_{2\times2} & 0_{2\times2} & 0_{2\times2} & -R_{c_m} \end{bmatrix} \begin{bmatrix} \frac{\partial H_\zeta}{\partial \dot{q}_l} \\ \frac{\partial H_\zeta}{\partial \dot{q}_m} \\ \frac{\partial H_\zeta}{\partial \dot{p}_l} \\ \frac{\partial H_\zeta}{\partial \dot{p}_m} \\ \frac{\partial H_\zeta}{\partial \dot{x}_{c_l}} \\ \frac{\partial H_\zeta}{\partial \dot{x}_{c_m}} \end{bmatrix} \tag{4.21}$$

Alternatively, the closed loop system described in (4.21) can be written in a compact form:

$$\dot{\zeta} = F_\zeta \frac{\partial H_\zeta}{\partial \zeta}. \tag{4.22}$$

From (2.15) we know that F_ζ must allow a decomposition into a skew-symmetric interconnection matrix J and a symmetric positive semi-definite damping matrix R, such that $F_\zeta = J - R$. Thus, decomposing F_ζ into a symmetric and a skew-symmetric part according to $F_\zeta = \frac{1}{2}(F_\zeta + F_\zeta^\top) + \frac{1}{2}(F_\zeta - F_\zeta^\top)$, we obtain the following symmetric matrix

$$\frac{1}{2}(F_\zeta + F_\zeta^\top) = \begin{bmatrix} 0_{2\times2} & 0_{2\times2} & 0_{2\times2} & 0_{2\times2} & 0_{2\times2} & 0_{2\times2} \\ 0_{2\times2} & 0_{2\times2} & 0_{2\times2} & 0_{2\times2} & 0_{2\times2} & 0_{2\times2} \\ 0_{2\times2} & 0_{2\times2} & -D_l & 0_{2\times2} & \frac{1}{2}I_{2\times2} & 0_{2\times2} \\ 0_{2\times2} & 0_{2\times2} & 0_{2\times2} & -D_m & -\frac{1}{2}I_{2\times2} & 0_{2\times2} \\ 0_{2\times2} & 0_{2\times2} & \frac{1}{2}I_{2\times2} & -\frac{1}{2}I_{2\times2} & -R_{c_l} & 0_{2\times2} \\ 0_{2\times2} & 0_{2\times2} & 0_{2\times2} & 0_{2\times2} & 0_{2\times2} & -R_{c_m} \end{bmatrix} \tag{4.23}$$

Using the condition given in (4.4), it can be shown that $\frac{1}{2}(F_\zeta + F_\zeta^\top) \leq 0$, thus proving that (4.21) satisfies the geometric structure of the pH-form.

The third and last point to prove is that of global asymptotic stability of the closed-loop system. To this end, H_ζ from (4.10) is used as a Lyapunov function. First, it is shown that H_ζ is non-increasing

$$\dot{H}_\zeta = \left(\frac{\partial H_\zeta}{\partial \zeta}\right)^\top \dot{\zeta} = \left(\frac{\partial H_\zeta}{\partial \zeta}\right)^\top F_\zeta \frac{\partial H_\zeta}{\partial \zeta} \leq 0 \tag{4.24}$$

and it is observed that, since

$$z_{l_*} = z_{m_*} = 0_2 \quad \Longrightarrow \quad \left(\frac{\partial \phi_l}{\partial q_l}\right)_* = \left(\frac{\partial \phi_l}{\partial x_{c_l}}\right)_* = \left(\frac{\partial \phi_m}{\partial q_m}\right)_* = \left(\frac{\partial \phi_m}{\partial x_{c_m}}\right)_* = 0_2 \tag{4.25}$$

it can be stated that

$$\left(\frac{\partial H_\zeta}{\partial \zeta}\right)_* = 0_{12}. \tag{4.26}$$

Thus, the Lyapunov function H_ζ is a non-increasing function, and its derivative equals zero at the equilibrium. Now to state that the equilibrium point is at a minimum of the Lyapunov function, it must be shown that the value of the second derivative evaluated at the equilibrium is positive.

$$\left(\frac{\partial^2 H_\zeta}{\partial \zeta^2}\right) = \begin{bmatrix} \frac{\partial^2 H_\zeta}{\partial q_l^2} & \frac{\partial^2 H_\zeta}{\partial q_l\, \partial q_m} & \frac{\partial^2 H_\zeta}{\partial q_l\, \partial p_l} & \frac{\partial^2 H_\zeta}{\partial q_l\, \partial p_m} & \frac{\partial^2 H_\zeta}{\partial q_l\, \partial x_{c_l}} & \frac{\partial^2 H_\zeta}{\partial q_l\, \partial x_{c_m}} \\ \frac{\partial^2 H_\zeta}{\partial q_m\, \partial q_l} & \frac{\partial^2 H_\zeta}{\partial q_m^2} & \frac{\partial^2 H_\zeta}{\partial q_m\, \partial p_l} & \frac{\partial^2 H_\zeta}{\partial q_m\, \partial p_m} & \frac{\partial^2 H_\zeta}{\partial q_m\, \partial x_{c_l}} & \frac{\partial^2 H_\zeta}{\partial q_m\, \partial x_{c_m}} \\ \frac{\partial^2 H_\zeta}{\partial p_l\, \partial q_l} & \frac{\partial^2 H_\zeta}{\partial p_l\, \partial q_m} & \frac{\partial^2 H_\zeta}{\partial p_l^2} & \frac{\partial^2 H_\zeta}{\partial p_l\, \partial p_m} & \frac{\partial^2 H_\zeta}{\partial p_l\, \partial x_{c_l}} & \frac{\partial^2 H_\zeta}{\partial p_l\, \partial x_{c_m}} \\ \frac{\partial^2 H_\zeta}{\partial p_m\, \partial q_l} & \frac{\partial^2 H_\zeta}{\partial p_m\, \partial q_m} & \frac{\partial^2 H_\zeta}{\partial p_m\, \partial p_l} & \frac{\partial^2 H_\zeta}{\partial p_m^2} & \frac{\partial^2 H_\zeta}{\partial p_m\, \partial x_{c_l}} & \frac{\partial^2 H_\zeta}{\partial p_m\, \partial x_{c_m}} \\ \frac{\partial^2 H_\zeta}{\partial x_{c_l}\, \partial q_l} & \frac{\partial^2 H_\zeta}{\partial x_{c_l}\, \partial q_m} & \frac{\partial^2 H_\zeta}{\partial x_{c_l}\, \partial p_l} & \frac{\partial^2 H_\zeta}{\partial x_{c_l}\, \partial p_m} & \frac{\partial^2 H_\zeta}{\partial x_{c_l}^2} & \frac{\partial^2 H_\zeta}{\partial x_{c_l}\, \partial x_{c_m}} \\ \frac{\partial^2 H_\zeta}{\partial x_{c_m}\, \partial q_l} & \frac{\partial^2 H_\zeta}{\partial x_{c_m}\, \partial q_m} & \frac{\partial^2 H_\zeta}{\partial x_{c_m}\, \partial p_l} & \frac{\partial^2 H_\zeta}{\partial x_{c_m}\, \partial p_m} & \frac{\partial^2 H_\zeta}{\partial x_{c_m}\, \partial x_{c_l}} & \frac{\partial^2 H_\zeta}{\partial x_{c_m}^2} \end{bmatrix} \tag{4.27}$$

Calculating most of these partial derivatives is straightforward, and many simply equal zero when they are evaluated at the equilibrium. Furthermore, note that

$$\begin{aligned} \frac{\partial^2 \phi_l}{\partial q_l^2} &= \frac{\partial^2 \phi_l}{\partial x_{c_l}\, \partial q_l} = \frac{\partial^2 \phi_l}{\partial q_l\, \partial x_{c_l}} = \frac{\partial^2 \phi_l}{\partial x_{c_l}^2} \\ &= \begin{bmatrix} \beta_{l_1}\alpha_{l_1} \operatorname{sech}^2 \beta_{l_1} z_{l_1} & 0 \\ 0 & \beta_{l_2}\alpha_{l_2} \operatorname{sech}^2 \beta_{l_2} z_{l_2} \end{bmatrix}, \\ \frac{\partial^2 \phi_m}{\partial q_m^2} &= \frac{\partial^2 \phi_m}{\partial x_{c_m}\, \partial q_m} = \frac{\partial^2 \phi_m}{\partial q_m\, \partial x_{c_m}} = \frac{\partial^2 \phi_m}{\partial x_{c_m}^2} \\ &= \begin{bmatrix} \beta_{m_1}\alpha_{m_1} \operatorname{sech}^2 \beta_{m_1} z_{m_1} & 0 \\ 0 & \beta_{m_2}\alpha_{m_2} \operatorname{sech}^2 \beta_{m_2} z_{m_2} \end{bmatrix} \end{aligned} \tag{4.28}$$

Evaluating (4.27) at the equilibrium ζ_* yields

$$\left(\frac{\partial^2 H_\zeta}{\partial \zeta^2}\right)_* = \begin{bmatrix} K_s + A_l & -K_s & 0_2 & 0_2 & A_l & 0_2 \\ -K_s & K_s + A_m & 0_2 & 0_2 & 0_2 & A_m \\ 0_2 & 0_2 & M_{l_*}^{-1} & 0_2 & 0_2 & 0_2 \\ 0_2 & 0_2 & 0_2 & M_{m_*}^{-1} & 0_2 & 0_2 \\ A_l & 0_2 & 0_2 & 0_2 & A_l & 0_2 \\ 0_2 & A_l & 0_2 & 0_2 & 0_2 & A_m + K_c \end{bmatrix} > 0 \tag{4.29}$$

where we should recall that K_s, M_l and M_m are the matrices for the spring constant and mass inertia's for links and motors respectively, given in the model

description in Chapter 3. Furthermore, K_c is a control parameter, and A_l and A_m are defined as

$$\begin{aligned} A_l &= \begin{bmatrix} \beta_{l_1}\alpha_{l_1} & 0 \\ 0 & \beta_{l_2}\alpha_{l_2} \end{bmatrix} \\ A_m &= \begin{bmatrix} \beta_{m_1}\alpha_{m_1} & 0 \\ 0 & \beta_{m_2}\alpha_{m_2} \end{bmatrix} \end{aligned} \tag{4.30}$$

Thus, since the H_ζ is used as a Lyapunov function, its derivative is non-increasing and equals zero at the equilibrium point, and its second derivative is positive indicating that the equilibrium point is in fact a minimum, it can be concluded that the system is stable in the sense of Lyapunov. To prove asymptotic stability using Barbashin's theorem, it need only be determined that $\dot{H}_\zeta = 0$ if and only if $\zeta = \zeta_*$

Note that

$$\begin{aligned} \dot{H}_\zeta = 0 \iff & \begin{cases} \frac{\partial H_\zeta}{\partial q_m} = 0_2 \implies -K_s(q_l - q_m) + \frac{\partial \phi_m}{\partial q_m} = 0_2 \\ \frac{\partial H_\zeta}{\partial p} = 0_4 \implies p = 0_4 \\ \frac{\partial H_\zeta}{\partial x_{c_l}} = 0_2 \implies \frac{\partial \phi_l}{\partial x_{c_l}} = 0_2 \implies \frac{\partial \phi_l}{\partial q_l} = 0_2 \implies z_l = 0_2 \\ \frac{\partial H_\zeta}{\partial x_{c_m}} = 0_2 \implies K_c x_{c_m} + \frac{\partial \phi_m}{\partial x_{c_m}} = 0_2 \end{cases} \\ \implies & \begin{cases} \frac{\partial H_\zeta}{\partial q_l} = 0_2 \implies K_s(q_l - q_m) = 0_2 \implies q_l = q_m \\ \frac{\partial \phi_m}{\partial q_m} = 0_2 \implies z_m = 0_2 \text{ and } x_{c_m} = 0_2 \\ q_l = q_m = q_* \\ x_{c_l} = 0_2 \end{cases} \end{aligned} \tag{4.31}$$

Thus, the closed-loop system is asymptotically stable.

It can be shown that H_ζ is radially unbounded, when we recall that

$$\begin{aligned} H_\zeta &= H + \phi_l + \phi_m + \frac{1}{2} x_{c_m}^\top K_c x_{c_m} \\ \text{with} \quad H &= \frac{1}{2} p^\top M^{-1} p + \frac{1}{2}(q_l - q_m)^\top K_s (q_l - q_m) \\ \text{and} \quad \phi_l &:= \sum_{i=1}^{2} \frac{\alpha_{l_i}}{\beta_{l_i}} \ln\left(\cosh\left(\beta_{l_i}(q_l - q_* + x_{c_l})\right)\right) \\ \text{and} \quad \phi_m &:= \sum_{i=1}^{2} \frac{\alpha_{m_i}}{\beta_{m_i}} \ln\left(\cosh\left(\beta_{m_i}(q_m - q_* + x_{c_m})\right)\right) \end{aligned} \tag{4.32}$$

[ht]

$H_\zeta(\zeta)$ is radially unbounded, because

$$||\zeta|| \to \infty \quad \Longrightarrow \quad H_\zeta(\zeta) \to \infty \tag{4.33}$$

Thus, we can conclude that the closed-loop system is globally asymptotically stable. □

Control parameters and controller behavior

The first important aspect of the controller follows from (4.4), which states that $R_{c_l} > \frac{1}{4}(D_l^{-1} + D_m^{-1})$, which acts as a lower bound for the Lyapunov stability property. Here, the importance of the D_l and D_m parameters is evident, since lower parameters result in a higher lower bound for R_{c_l}. Using the parameters from 3.1 results in a lower bound for $R_{c_l} > diag\{1.6, 5.7\}$.

Recall (4.5), which can be compactly written as $u = u_l + u_m$. When only one joint is considered, u_l and u_m can simply be written as:

$$\begin{aligned} u_l &= -\alpha_l \tanh(\beta z_l), \qquad & z_l &= q_l - q_* + x_{c_l} \\ u_m &= -\alpha_m \tanh(\beta_m z_m), & z_m &= q_m - q_* + x_{c_m} \end{aligned} \tag{4.34}$$

Within u_l and u_m, the α-parameters are the maximum value of that specific element of the controller, and the corresponding β-parameters regulate how quickly this value is reached. In other words, the values for α_l and α_m determine how much weight that controller element has in the control signal. Moreover, the controller-elements are based on z-variables, whose values depend on the state of the system.

When the z-parameters are large and positive, for instance when $q_l, q_m >> q_*$, then the control signal becomes large in the opposite direction, driving q_m and q_l faster towards q_*. The z-variables depend on x_{c_l} and x_{c_m} as well, which are virtual states that are implemented to inject the damping into the movements. Again, when only regarding one joint, the dynamics of these virtual states can be written as:

$$\begin{aligned} \dot{x}_{c_l} &= -R_{c_l}\big(\alpha_l \tanh(\beta z_l)\big) \\ \dot{x}_{c_m} &= -R_{c_m}\big(\alpha_m \tanh(\beta_m z_m) + K_c x_{c_m}\big) \end{aligned} \tag{4.35}$$

Clearly, x_{c_l} decreases when z_l is positive and vice versa, and the rate of this change is determined by R_{c_l} and α_l. Through its definition, $|z_l|$ decreases due to the change in x_{c_l}. This propagates back into the control signal, whose magnitude decreases. Thus, the presence of x_{c_l} will always have a diminishing effect on the control signal. When R_{c_l} is chosen very high, x_{c_l} changes rapidly towards a value where z_l close to zero, at which point the control element u_l becomes close to zero as well. When R_{c_l} is chosen very low, x_{c_l} changes very slowly and u_l is damped

too little, leading to larger oscillations. Recall that the value for R_{c_l} must always satisfy the lower bound given by (4.4).

The damping effect of x_{c_m} is similar to x_{c_l}, but involves an additional term $K_c x_{c_m}$. This means that when x_{c_m} increases or decreases, its rate of change is lowered automatically. It can be expected that because of this, x_{c_m} reacts slower and with smaller magnitude than x_{c_l}, and in turn, the damping of u_m becomes less strong.

To summarize these observations regarding the controller behavior, it can be said that

- α_l is the maximum signal value for u_l,
- β_l regulates how quickly u_l adapts, based on z_l,
- R_{c_l} impacts how strongly u_l is damped
- α_m is the maximum signal value for u_m,
- β_m regulates how quickly u_m adapts, based on z_m,
- R_{c_m} impacts how strongly u_m is damped
- K_c diminishes rate of change for x_{c_m}, limiting the damping effect of R_{c_m}

4.2 Saturated control with integral action

The naturally saturated control law that was given in the previous section can be adapted to take into account an extra state, that acts as an *integral* term of the error signal.

In Proposition 4.2.1, the new state $\sigma \in \mathbb{R}^2$ will be used to apply integral action in the controller to eliminate the steady state error. This control law was first proposed and proven in [5] as well.

Proposition 4.2.1. *Let the new state $\sigma \in \mathbb{R}^2$ follow the dynamics*

$$\dot{\sigma} = \frac{\partial^2 \phi_\sigma}{\partial \sigma^2}(\sigma)(q_m - q_*) - K_\sigma \sigma \tag{4.36}$$

where K_σ and the ϕ_σ are defined as

$$\begin{aligned} \phi_\sigma(\sigma) &:= \sum_{i=1}^{2} \frac{\alpha_{\sigma_i}}{\beta_{\sigma_i}} \ln\left(\cosh\left(\beta_{\sigma_i}\sigma_i\right)\right) \\ K_\sigma &:= diag\{k_{\sigma_1}, k_{\sigma_2}\} \end{aligned} \tag{4.37}$$

with $\alpha_{\sigma_i}, \beta_{\sigma_i}, k_{\sigma_i} \in \mathbb{R}_{\geq 0}$ for $i = 1, 2$.

Now, consider the control law

$$u = -\frac{\partial \phi_l}{\partial z_l}(z_l(q_l, x_{c_l})) - \frac{\partial \phi_m}{\partial z_m}(z_m(q_m, x_{c_m})) - \frac{\partial \phi_\sigma}{\partial \sigma}(\sigma). \tag{4.38}$$

where ϕ_l, ϕ_m, z_l and z_m are previously defined in (4.1) and (4.2). The reference point q_* is set and the following matrices are defined

$$\begin{aligned} A_\sigma &:= diag\{\beta_{\sigma_1}\alpha_{\sigma_1}, \beta_{\sigma_2}\alpha_{\sigma_2}\}; \\ A_{\xi_1} &:= \begin{bmatrix} 0_6 \\ -A_\sigma \\ 0_4 \end{bmatrix} \qquad A_{\xi_2} := \begin{bmatrix} 0_2 \\ A_\sigma \\ 0_8 \end{bmatrix} \\ \mathcal{A} &:= \begin{bmatrix} F_\zeta(\frac{\partial^2 H_\zeta}{\partial \zeta^2})_* & A_{\xi_1} \\ A_{\xi_2}^\top & -K_\sigma \end{bmatrix} \end{aligned} \tag{4.39}$$

with F_ζ and $(\frac{\partial^2 H_\zeta}{\partial \zeta^2})_*$ previously defined in (4.22) and (4.29).

Then:

1. *The control signal u given in (4.38) is naturally saturated.*
2. *The system (3.2) in closed-loop with (4.38) has an asymptotically stable equilibrium point $\xi_* =:= [\zeta^\top, \sigma^\top] = [q_*^\top, q_*^\top, 0_{10}^\top]$ if the matrix $\mathcal{A}$ is Hurwitz.*

Proof. Firstly, note that

$$\frac{\partial \phi_\sigma}{\partial \sigma} = \begin{bmatrix} \alpha_{\sigma_1} \tanh\left(\beta_{\sigma_1}\sigma_1\right) \\ \alpha_{\sigma_2} \tanh\left(\beta_{\sigma_2}\sigma_2\right) \end{bmatrix} \tag{4.40}$$

Using the proof of item 1 in Proposition 4.1.1 it is determined that

$$u_i = -\alpha_{l_i} \tanh\left(\beta_{l_i} z_{l_i}\right) - \alpha_{m_i} \tanh\left(\beta_{m_i} z_{m_i}\right) - \alpha_{\sigma_i} \tanh\left(\beta_{\sigma_i}\sigma_i\right). \tag{4.41}$$

Thus, it can be concluded that u_i is bounded by

$$-\left(\alpha_{l_i} + \alpha_{m_i} + \alpha_{\sigma_i}\right) \leq u_i \leq \alpha_{l_i} + \alpha_{m_i} + \alpha_{\sigma_i}. \tag{4.42}$$

Secondly, to proof item 2, the state space $\xi := [\zeta^\top \sigma^\top]^\top$ is defined, along with the error $\bar{\xi} := \xi - \xi_*$. The local stability of the closed loop system around the equilibrium point $\bar{\xi}_*$ can be established with Lyapunov's indirect method.

Note that from all dynamics from (4.21) the new control law (4.38) only affects $\dot{p}_m$, which is appended with $-\frac{\partial \phi_\sigma}{\partial \sigma}$.

The new closed-loop systems can be described as (4.21), appended with two extra columns and rows to include the new state σ. To express this new closed-loop system, two new matrices are defined:

$$F_{\xi_1} := \begin{bmatrix} 0_{6\times 2} \\ -\frac{\partial \phi_\sigma}{\partial \sigma} \\ 0_{4\times 2} \end{bmatrix} \qquad F_{\xi_2} := \begin{bmatrix} 0_{2\times 2} \\ \frac{\partial^2 \phi_\sigma}{\partial \sigma^2}(q_m - q_*) \\ 0_{8\times 2} \end{bmatrix} \tag{4.43}$$

The closed-loop system can be described by

$$\mathcal{F}_\xi := \begin{bmatrix} F_\zeta\left(\frac{\partial H_\zeta}{\partial \zeta}\right) & F_{\xi_1} \\ F_{\xi_2}^\top & -K_\sigma \sigma \end{bmatrix} \tag{4.44}$$

Now for the linearization, the Jacobian of $\mathcal{F}_\xi$ is calculated and evaluated at the equilibrium point.

$$\mathcal{A} := \frac{\partial \mathcal{F}_\xi}{\partial \xi}\bigg|_{\bar{\xi}=\bar{\xi}_*} = \begin{bmatrix} F_\zeta(\frac{\partial^2 H_\zeta}{\partial \zeta^2}) & \frac{\partial F_{\xi_1}}{\partial \sigma} \\ \frac{\partial A_{\xi_2}^\top}{\partial \zeta} & -K_\sigma \end{bmatrix}_{\bar{\xi}=\bar{\xi}_*} = \begin{bmatrix} F_\zeta(\frac{\partial^2 H_\zeta}{\partial \zeta^2})_* & A_{\xi_1} \\ A_{\xi_2}^\top & -K_\sigma \end{bmatrix} \tag{4.45}$$

Calculations of the eigenvalues of this matrix $\mathcal{A}$ show that their real values are all negative, thus the linearized system is asymptotically stable and the corresponding nonlinear system is determined to be locally asymptotically stable. □

Control parameters and controller behavior

Recall (4.38), which can be compactly written as $u = u_l + u_m + u_\sigma$. The parameters that are involved in u_l and u_m have already been discussed in Section 4.1, so here the focus will be on u_σ.

When only one joint is considered, u_σ can simply be written as:

$$u_\sigma = -\alpha_\sigma \tanh(\beta_\sigma \sigma) \tag{4.46}$$

Firstly, it is evident that u_σ-signal becomes stronger for a higher α_σ, β_σ and σ. Again, α_σ and β_σ are set control parameters, and σ follows the dynamics that are shown in (4.36), which can, looking at a single joint, be written as:

$$\dot{\sigma} = \alpha_\sigma \beta_\sigma \operatorname{sech}^2(\beta_\sigma \sigma)(q_m - q_*) - K_\sigma \sigma \tag{4.47}$$

where $sech^2(x)$ has the form that is shown in Figure 4.2.

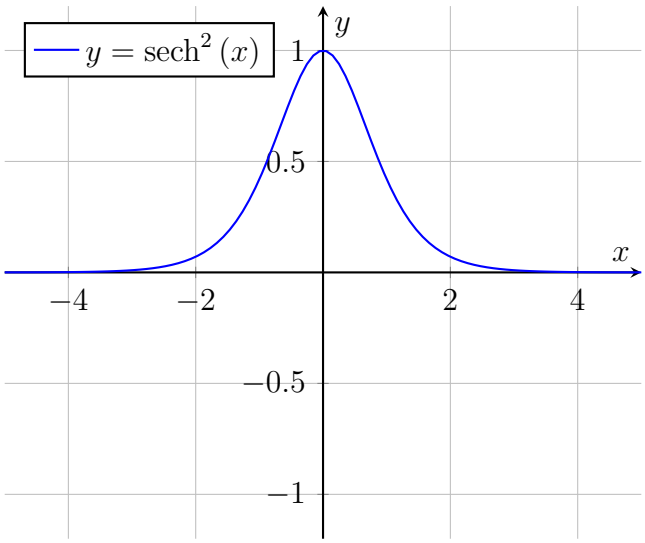

Figure 4.2: Plot of the $\operatorname{sech}^2(x)$ function

Thus, based on this form, when σ is close to 0, it changes more rapidly, and when σ is further to 0 its rate of change is smaller. Furthermore, $|\sigma|$ increases more quickly as the difference $|q_m - q_*|$ increases. Finally, the term $K_\sigma \sigma$ has a limiting, damping effect on the rate of change in σ. This limiting effect becomes stronger when σ increases, ultimately leading to a decrease of σ.

The u_σ element of the controller functions as an integral action, because it acts as an integral over the positional error $q_m - q_*$. Hence, equal to the use of the integral action in a PID-controller, the u_σ-element is used to remove the steady state error.

The behavior of the control parameters related to u_l and u_m is not changed by the addition of this extra control element. The addition of u_l is an extension

to the controller that increases its performance. To conclude, the behavior of the parameters within u_σ can be summarized as follows,

- α_σ is the maximum signal value for u_σ,
- β_σ regulates how quickly u_σ adapts,
- K_σ diminishes rate of change for σ

Chapter 5

Experiment design and setup

In this chapter, the pick and place routine is presented, and the two different approaches that will be used are explained. In one approach, the movements will be based on time, and in the other approach the movements are based on the joint positions.

In the time-based approach, each movement has a predetermined time in which the robotic arm should converge to its desired position. In this way, the timing of the movements of the robotic arm is consistent during each iteration; each picking movement and placing movement can timed exactly. However, it may happen that the convergence of the positions is not entirely accurate within the predetermined time. Such a consistently timed routine can be useful if it is implemented into a system that requires this kind of regularity in the output.

For the position-based approach, the next step in the routine only starts when the current movement has reached its desired position. In this approach, the accuracy of the movements is guaranteed, but the timing of the convergence to the desired positions can be irregular. If the timing is less important than the accuracy, the position-based approach is better suited than the time-based approach.

5.1 The pick and place routine

In both approaches, the system will move from an initial position (q_0), to a pick-position (q_{pick}) and to a place-position (q_{place}). This picking and placing routine can be repeated a few cycles after which the system returns to its initial position. At the pick-position, the end-effector of the robotic arm is used to pick up a small paper cup. The paper cup is then moved towards the place-position, where it is dropped into a stack of paper cups. The reference points for q_0, q_{pick} and q_{place} are the joint angles in radians and are defined as

$$\begin{aligned} q_0 &= (0,\ 0) \\ q_{pick} &= (\text{-}0.2,\ \text{-}0.5) \\ q_{place} &= (0.8,\ 0.4) \end{aligned}$$

Figure 5.1 shows how these angles correspond with the actual position of the

robotic arm.

(a) In the q_{place} position (b) In the q_0 position (c) In the q_{pick} position

Figure 5.1: The Quanser Robotic arm in the three different positions

The placing action requires a higher accuracy than the picking action. To succesfully achieve the placing action, the position of the end-effector must be within 12[mm] of the reference point. This corresponds to a maximum error in the angular position of about 0.015 radians for the first joint and about 0.035 radians for the second joint. The method of calculating the positional error of the end-effector based on the joint angles can be found in Appendix A.

To determine whether each controller can achieve the desired accuracy in the end-effector position, the time-based experiment is first performed without the picking and placing of the cup. If the required accuracy can be achieved, the actual pick and place experiments are performed.

Time-based routine

In the time-based routine, each new movement is instigated after a given amount of time, which ensures a consistent timing of the movements. The setpoint regulation experiments from [19] indicate that for both controllers, the steady state can usually be achieved within 7 seconds. To introduce some slack in the movements, a maximum time to reach the desired position for each movement is set to 10 seconds. This way, it can be expected that the positions are converged before the next movement begins. Following the structure of 3 picking movements, 3 placing movements and a return to the initial position, the complete procedure without end-effector will take 70s.

When the end-effector is included as well, each movement is extended with 2 seconds to incorporate the opening and closing action. The time scheme for this pick and place routine is given in Table 5.1.

Time	Action
0s	move towards q_{pick}
10s	close end-effector
12s	move towards q_{place}
22s	open end-effector
24s	move towards q_{pick}
34s	close end-effector
36s	move towards q_{place}
46s	open end-effector
48s	move towards q_{pick}
58s	close end-effector
60s	move towards q_{place}
70s	open end-effector
72s	move towards q_0
82s	routine is finished

Table 5.1: Time-scheme for the time-based routine

Position-based routine

In the position-based routine, the position measurements are used to determine when the next movement must begin. The end-effector only opens and closes when it is within the range of 10mm around the desired position, and the arm only moves when the end-effector has gripped the cup if it is opened fully. This way, the precision of the movement is ensured, but there may be inconsistencies in the timing of the movements.

Trigger	Action
Start of routine	Move towards q_{pick}
End-effector within accuracy limits	Close end-effector
End-effector is closed	Move towards q_{place}
End-effector within accuracy limits	Open end-effector
End-effector is open	Move end-effector to picking position

Practical challenges

The routine is a more demanding task than a setpoint regulation as performed in [19, 5], as it involves small and large movements in both directions. This can expose new practical challenges that remain unseen in a setpoint regulation, such as motor asymmetry and integral windup.

Other issues that were encountered during the experiments are for instance, nonlinear friction, hysteresis and measurement uncertainties. Below, these phenomena and how they influence controller performance are described.

Friction The static friction that needs to be overcome to instigate a movement is higher than the friction when the arm is moving. When the initial static fric-

tion is overcome, the friction decreases. Then, when the velocity increases, the friction force increases as well. The dip in the friction coefficient at lower velocities is calles the Stribeck-effect. This is shown in Figure 5.2a.

Motor asymmetry Additional to the friction that is described above, it was observed that the behavior of the DC-motor differs based on the direction of its movement. For the first link, movement in the positive direction requires lower input signal than movement in the negative direction. This means that a controller that is tuned to perfectly perform a movement to a desired setpoint x, can exhibit poorer performance when the setpoint is changed to its negative, $-x$.

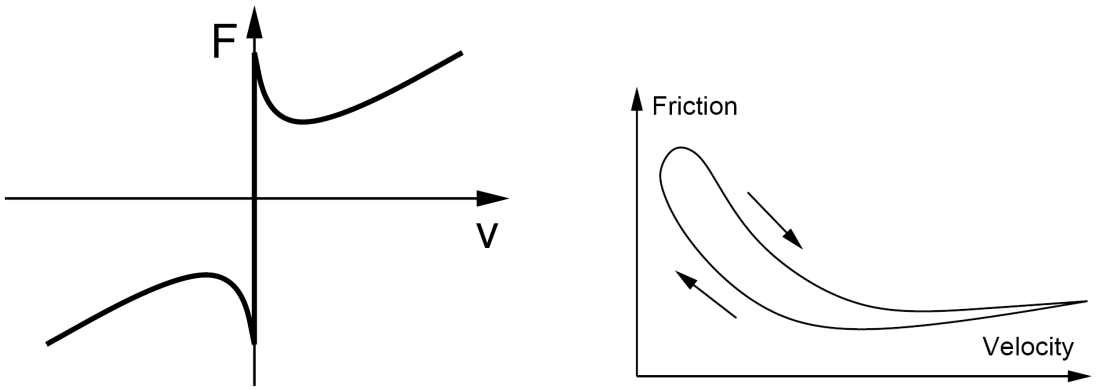

(a) Friction force as function of velocity

(b) Hysteresis loop

Figure 5.2: Examples of practical challenges that can occur during the experiments.

Hysteresis Another phenomenon that is related to the friction is a hysteresis in the relation between velocity and friction. Hysteresis means that the state of a system depends on its history, meaning that a certain input can have different outputs, depending on the previous inputs. In this case, it means that a certain velocity can result in different friction forces. Specifically, the friction force in decreasing velocities is lower than the friction force in increasing velocities, which is shown in Figure 5.2b.

Measurement uncertainty It has occurred that the DC-motors in the robotic arm *slip*, meaning that the position measurements from the motor show a movement when in fact there is none. In other words, the DC-motor rotates, but the rotation is not transferred to the arm, leading to incorrect measurements.

Integral windup When the controller uses an integral term to avoid a steady state error, it is possible that the value of this integral accumulates when

the system is moving towards a new setpoint. When the desires setpoint is reached, the value of the integral term may have become very high, leading to an excessive overshoot. This is called integral windup. Oftentimes, this effect can be reduced by tuning the different gains in the controller to ensure that the integral term does not become too high.

These phenomena can be difficult to model, and are not taken into account in the simulations. Their effects however can be noticed in the experimental results, which will be discussed in the following chapter.

Chapter 6

Results

In this chapter the results from testing the controllers on the proposed pick and place routine will be discussed.

In the first section, it is shown that the viscous friction parameters that were used in literature [14, 5] do not represent the damping parameters in the model for the robotic arm very well, leading to dissimilarities between the simulations and experiments. New parameter-estimates for the friction are calculated to decrease these dissimilarities.

The second and third section will present the results for the controllers from Sections 4.1 and 4.2 respectively. Both controllers will first be tested on their accuracy in a time-based routine without using the end-effector. When the experimental results show that the controller can achieve the desired accuracy, the end-effector will be added to the experiment. With the end-effector included, the position-based routine will be performed and their results are discussed.

Additionally, an analysis is done on the tunable parameters and the effect of different values on the performance of the control law.

6.1 Parameter identification for D_l and D_m

Performing the first simulations with the model parameters that were retrieved from the literature revealed that the convergence of the first joint is unexpectedly slow.

In Figure 6.1, the joint 1 positions in a time-based routine are shown, comparing experimental results with simulation results. The same control parameters are used in both results.

The simulation shows a very slow movement of the first joint, which is very dissimilar to the experimental results, where the movement is quick. Additionally, the large oscillations in the experimental results are absent in the simulation.

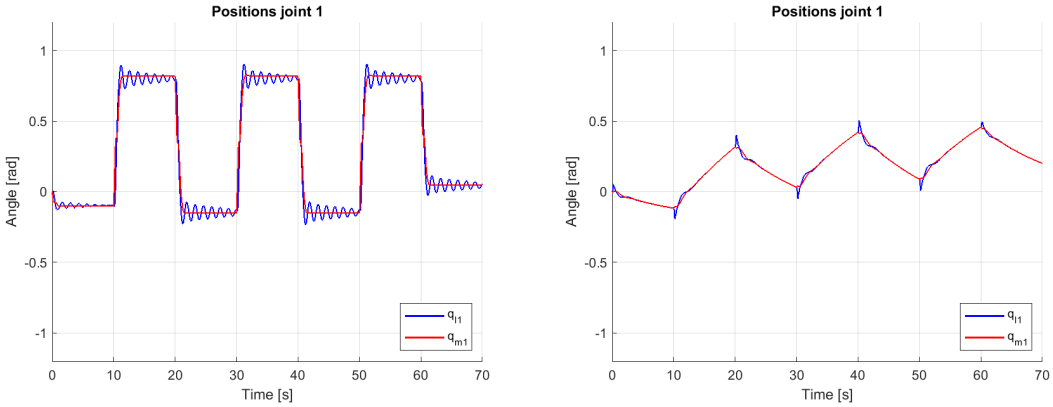

(a) Experimental results joint 1 (b) Simulation results joint 1

Figure 6.1: Joint 1 positions in experiment and simulation

In Figure 6.2 the same comparison for joint 2 is shown. The results for the second joint look rather similar. In the simulation, the first movement does not have a steady state error, the overshoots are slightly larger, and the small oscillations from the experiment are not present in the simulations.

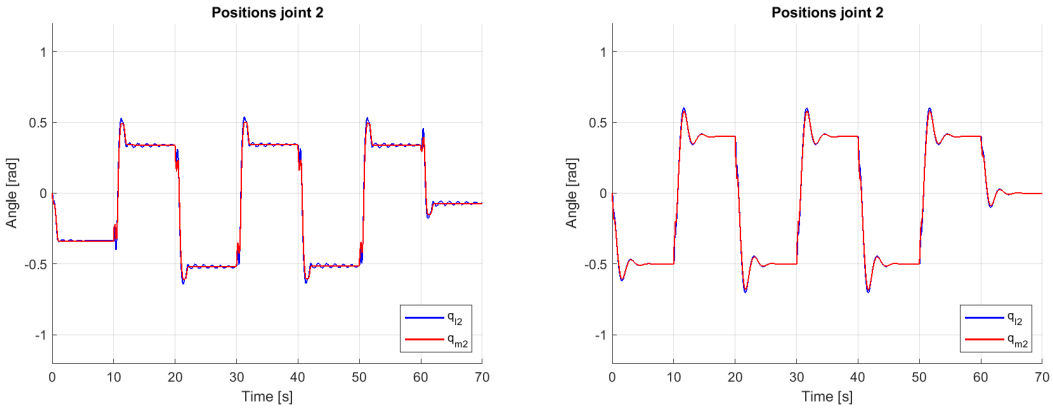

(a) Experimental results joint 2 (b) Simulation results joint 2

Figure 6.2: Joint 2 positions in experiment and simulation

These differences indicate that certain model parameters that are used in the simulations are inaccurate. Since the model parameters that were taken from the Quanser Reference Manual are assumed to be reliable, the values for D_l and D_m that were taken from [14] are more likely to cause the dissimilarities.

These values are given in Table 6.1. In [14], they describe the viscous friction and they are used together with coulomb friction parameters. In [5], they are used in the damping matrices, for which they are likely not very suitable.

Since the damping parameters are important for the lower bound on R_{c_l} as well, it would be beneficial to have better estimates for these parameters. Therefore, new estimates for these parameters are determined experimentally.

Parameter	Joint 1	Joint 2	unit
D_l	0.038	0.03	$[N \cdot m \cdot s/rad]$
D_m	8.435	0.136	$[N \cdot m \cdot s/rad]$

Table 6.1: Viscous friction parameters from [5, 14]

To calculate the parameters, the equations for the closed loop dynamics of the momenta are used, which are given below:

$$\begin{aligned} \dot{p}_l &= -\frac{\partial H}{\partial q_l} - D_l \frac{\partial H}{\partial p_l} \\ \dot{p}_m &= -\frac{\partial H}{\partial q_m} - D_m \frac{\partial H}{\partial p_m} + \tau \end{aligned} \tag{6.1}$$

These equations can easily be rewritten to

$$\begin{aligned} D_{l_i} &= \left(-\frac{\partial H}{\partial q_{l_i}} - \dot{p}_{l_i} \right) \frac{\partial H}{\partial p_{l_i}}^{-1} \\ D_{m_i} &= \left(-\frac{\partial H}{\partial q_{m_i}} + \tau_i - \dot{p}_{m_i} \right) \frac{\partial H}{\partial p_{m_i}}^{-1} \end{aligned} \tag{6.2}$$

where $i \in \{1, 2\}$ indicate the joint.

To calculate the partial derivatives of the Hamiltonian, the time-derivates $\dot{p}$ and $\dot{q}$ need to be determined during the experiment, which was done with a derivative filter. The input torque τ_i is calculated using the input signal u_i in [A] and the motor torque constant in [Nm/A] which is taken from the Quanser Reference Manual.

In the experiment, a constant input signal u is used to drive the motors, and the values for D_l and D_m are obtained as a time-series. The obtained data is then smoothened by using a moving average. The experiment was performed several times, with different input signals. The average of these values were taken and they are given in Table 6.2.

Parameter	Joint 1	Joint 2	unit
D_l	0.2	0.05	$[N \cdot m \cdot s/rad]$
D_m	0.7	0.3	$[N \cdot m \cdot s/rad]$

Table 6.2: Damping parameters that were obtained experimentally

To determine whether these new parameter values lead to better results, the simulations are performed again. The results are shown in Figure 6.3.

Clearly, the results for joint 1 are more similar to the experimental results from Figure 6.1. The convergences remains a bit slower, and the oscillations remain absent, but the overall form of the movements has improved much.

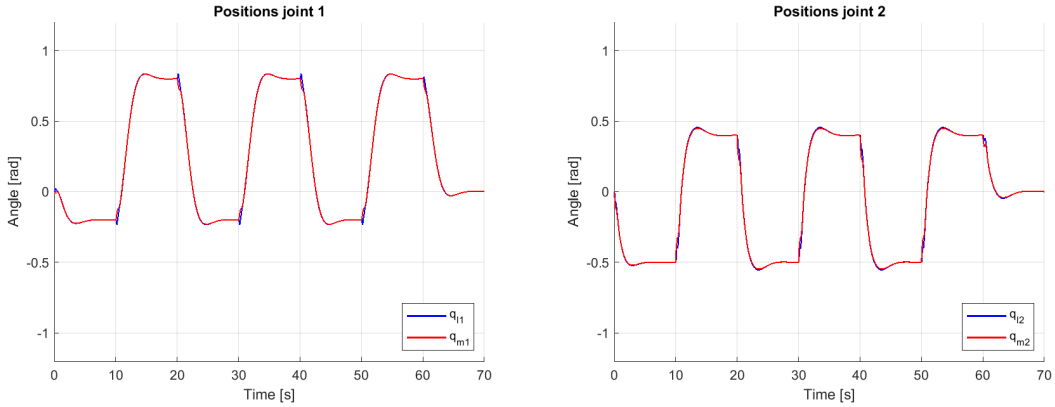

(a) Positions joint 1 (b) Positions joint 2

Figure 6.3: Simulated joint positions using the new damping parameters

For the second joint, the results did not change that much. The overshoot has decreased and the movements are a bit smoother. Compared to the experimental results, the overshoots were slightly larger at first, and with the new parameter values they are slightly lower.

Overall, it can be concluded that the new parameter values for D_l and D_m for the first joint are better suited than the parameter values from the literature. However, the simulation results remain somewhat dissimilar from the experimental results. The nonlinear friction in the robotic arm cannot be modelled adequately with these damping parameters. To better approach the experimental results, it would be better to include a non-linear friction model that also takes into account the static friction and coulomb friction. Also, other model parameters such as the moments of inertia, or the spring constants that are used in the simulation may not approximate the real system accurately.

6.2 Saturated control without velocity measurements

The controller from Section 4.1 will be tested, which is of the following form:

$$u_i = -\alpha_{l_i} \tanh\left(\beta_{l_i} z_{l_i}\right) - \alpha_{m_i} \tanh\left(\beta_{m_i} z_{m_i}\right) \tag{6.3}$$

where $i = 1, 2$ denotes the joint where the signal is applied. The dynamics of z_l and z_m can be found in 4.1 and 4.3

Experiment one

First, the following control parameters are set, which are used in both the experiment and the simulation.

$$
\begin{aligned}
R_{c_l} &= diag\{10, 40\}, & \alpha_{l_1} &= 0.7, & \alpha_{m_1} &= 0.24, \\
R_{c_m} &= diag\{25, 25\}, & \alpha_{l_2} &= 0.8, & \alpha_{m_2} &= 0.4, \\
K_c &= diag\{5, 5\}, & \beta_{l_1} &= 3, & \beta_{m_1} &= 2, \\
& & \beta_{l_2} &= 1.5, & \beta_{m_2} &= 1.5,
\end{aligned}
$$

Experimental results

The positions and control signals for both joints are shown in Figure 6.4. For both joints, the first movement does not attain its desired position, and there are small oscillations, which are stabilized within 10 seconds to reach a steady state.

The control signals for both joints start with a strong peak for each new movement, which then returns to a more or less constant value close to zero. After this peak in the signal, there is no more movement in the joints, apart from the oscillations.

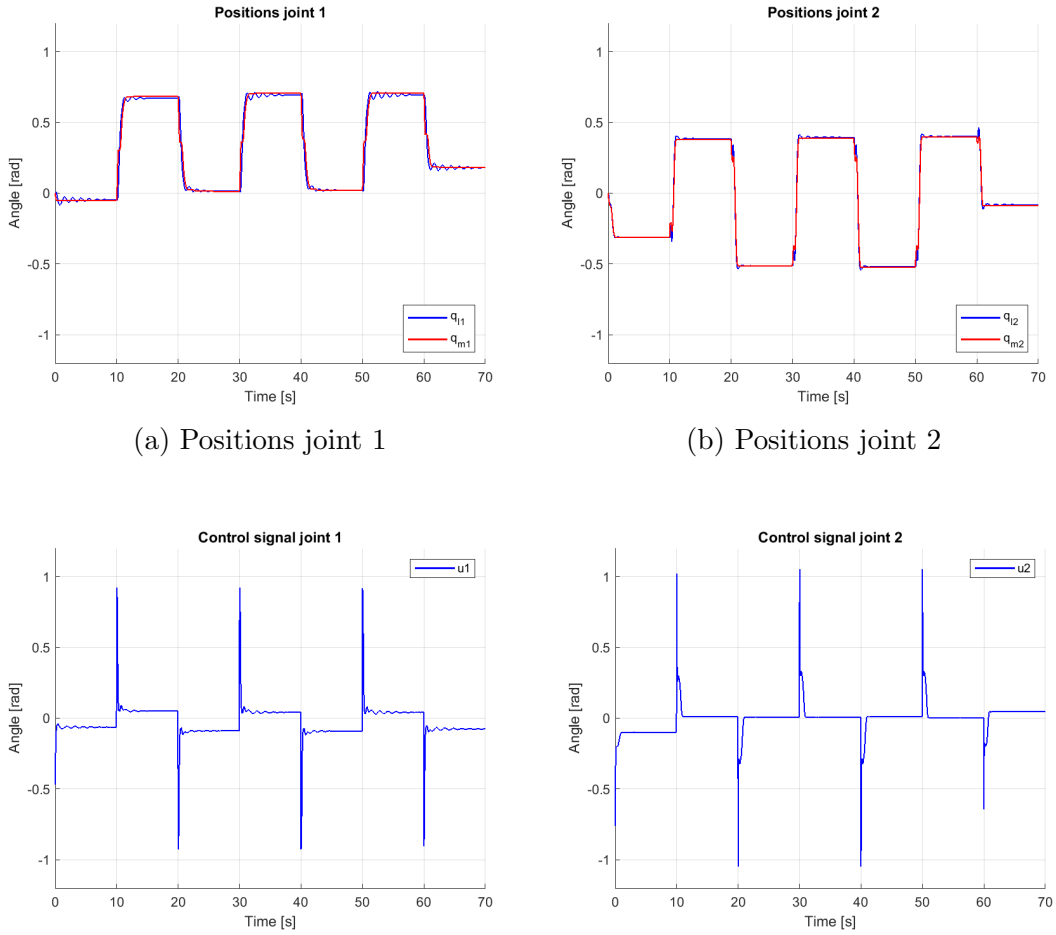

(a) Positions joint 1

(b) Positions joint 2

(c) Control signal joint 1

(d) Control signal joint 2

Figure 6.4: Positions and control signals for time-based experiment

For the first joint, there is a rather large steady state error in each movement,

which will result in the end-effector being far off the desired position. It is also striking that the error in the negative movement (towards $q_1 = -0.2$) is much larger than the error in the positive movement (towards $q_1 = 0.8$). This phenomenon can be attributed to the motor asymmetry; the motor in the first joint has more difficulties with the movements in the negative direction. The steady state errors in the first joint can also be seen in the control signals, where a nonzero signal remains. That this control signal is unable to move the motor, is because of the static friction

Apart from the first and last movement, the second joint seems to attain its reference position rather well. This is also reflected in the control signal that returns to zero in each movement. There are some irregularities in the positions at the beginning of each movement, that coincide with the acceleration in the first joint. The small oscillations of the second joint can be caused by the oscillations in the first joint.

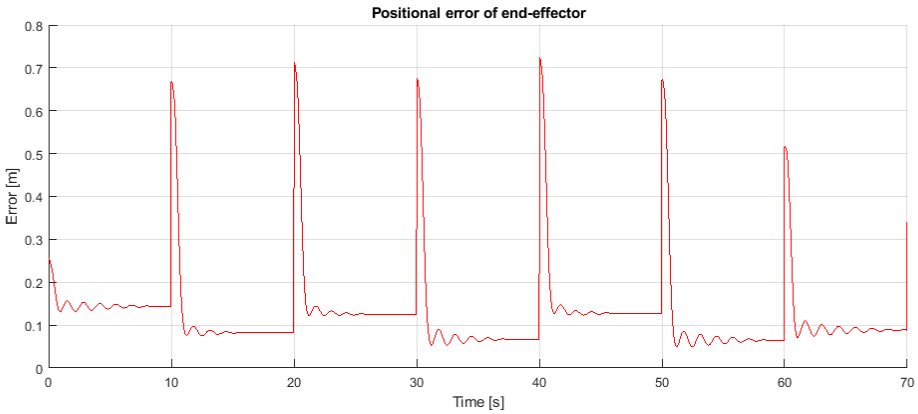

Figure 6.5: Positional error of end-effector

The positional error of the end-effector is shown in Figure 6.5. The error must be below 0.012[m] at the end of each movement to attain the needed accuracy, which is clearly not the case with the convergence around an error of 0.1[m]. The asymmetrical movements of the first joint become apparent here as well; the error during the second, fourth and sixth movements are lower than the rest.

From the non-zero control signals that are unable to move the arm, and the asymmetric convergence of the end-effector, it can be be concluded that the friction, especially the static friction, is a very important aspect.

It became clear during the experiments that for the first joint, control signals between $-0.12A < u < 0.10A$ cannot instigate or maintain a movement. For the second link, these values are $-0.11A < u < 0.11A$.

Ultimately, the steady state errors that are present in these experimental results prevent the end-effector of the arm to reach its desired position. Therefore, a change in control parameters will be made to try to better attain the desired accuracy.

Experiment two

To attempt to better attain the reference values in the first joint, the following control parameters are changed:

$$\alpha_{l_1} = 0.5, \qquad \alpha_{m_1} = 0.44,$$

Experimental results

The experimental results are shown in Figure 6.6.

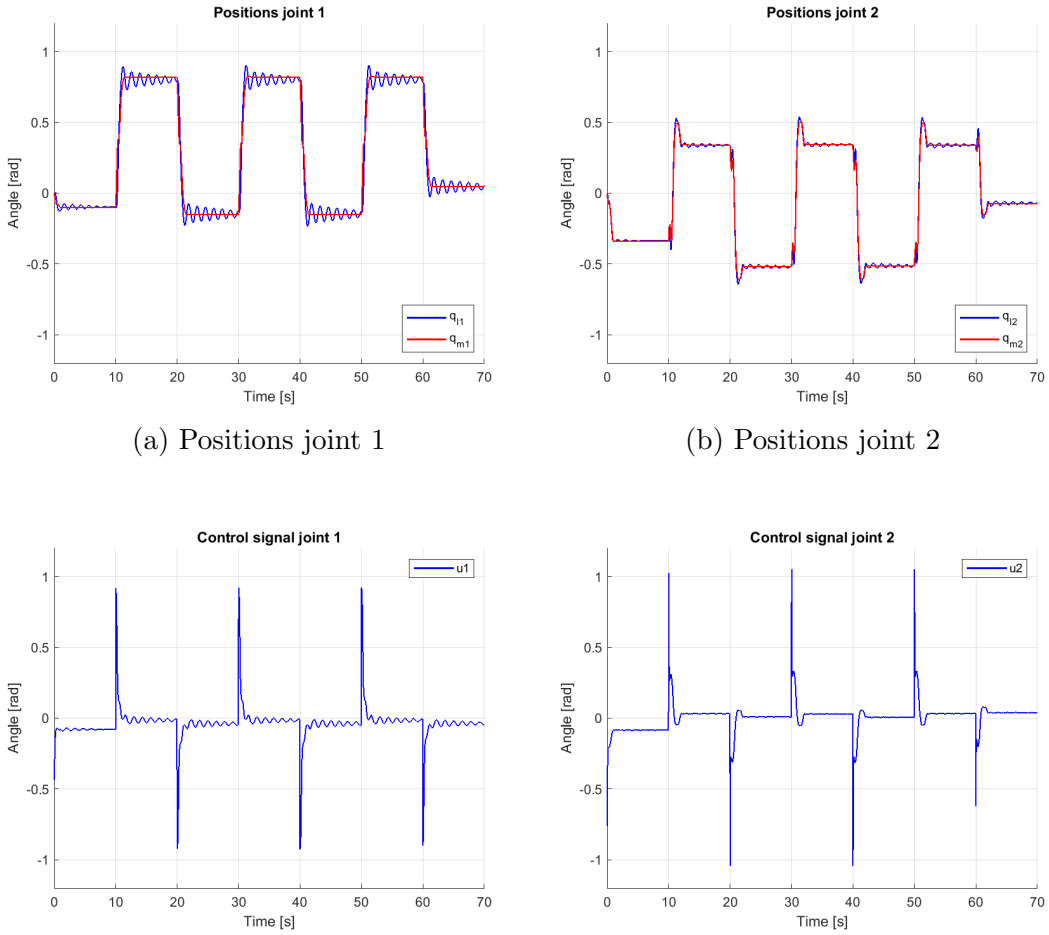

(a) Positions joint 1

(b) Positions joint 2

(c) Control signal joint 1

(d) Control signal joint 2

Figure 6.6: Positions for time-based experiment without gripper

The change in parameters results in a control signal that has a broader peak, which results in a bigger movement in the first joint. The first movement still does not come close to the desired position, but subsequent movements of joint 1 approach the reference position a lot better. However, the position measurements show very clear oscillations in the first joint, much worse than with the previous settings.

Additionally, the overshoot in the second joint has increased significantly. While in the previous result, the overshoot was difficult to distinguish from regular oscillation, it is very clear in this result that it is no regular oscillation due to the flexibility, because the motor angle overshoots as well now. Since the control parameters for the second joint were not changed, it can be concluded that the overshoot in the second joint is a result of the increased acceleration and deceleration in the first joint. This interaction between the links will make the second joint more difficult to control.

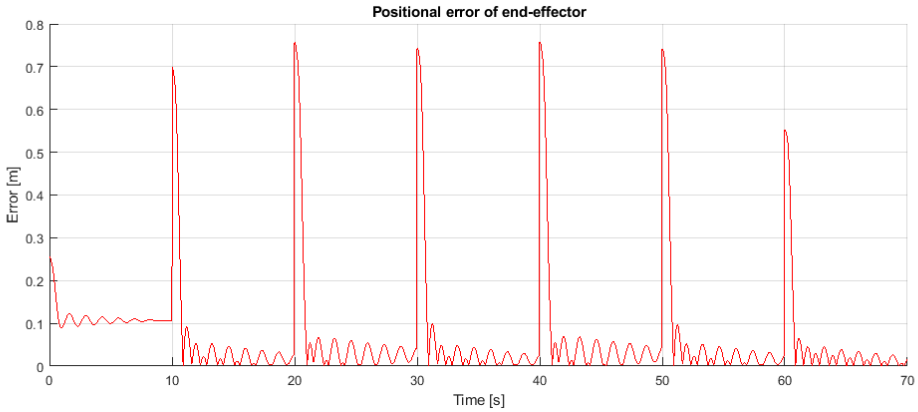

Figure 6.7: Positional error of the end-effector in meters

In Figure 6.7 the error in the end-effector is shown. While the overall error is lower for each movement, the stronger oscillations are clearly visible, and prevent the end-effector to remain within the desired accuracy bounds.

Conclusions

The experimental results that were discussed in this section showed that the control law from Section 4.1 is unable to attain the required level of accuracy.

Two different parameter configurations have been tested, which revealed a trade-off between a steady-state error and oscillations. The steady-state error can be reduced by increasing the gains for the motor, but this automatically means that the damping on the links is reduced, creating more oscillations.

Secondly, as long as the control signal remains low, for instance $-0.1A < u < 0.1A$, the static friction cannot be overcome and there will be no movements in the joints. Because of this, smaller movements such as the first movement in the routine, are more difficult to attain.

Thirdly, it was determined that the second joint was affected by the strong accelerations and decelerations of the first joint. This has a negative effect on the performance of the second joint, where it results in an overshoot.

6.3 Saturated control with integral action

Recall that the controller is of the following form

$$u_i = -\alpha_{l_i} \tanh\left(\beta_{l_i} z_{l_i}\right) - \alpha_{m_i} \tanh\left(\beta_{m_i} z_{m_i}\right) - \alpha_{\sigma_i} \tanh\left(\beta_{\sigma_i} \sigma_i\right) \tag{6.4}$$

where $i = 1, 2$ denotes the joint where the signal is applied. The dynamics of z_l and z_m can be found in 4.1 and 4.3

Time-based routine

First, the following control parameters are set.

$$\begin{array}{lllll} R_{c_l} = diag\{8, 50\}, & \alpha_{l_1} = 0.45, & \alpha_{l_2} = 0.2, & \beta_{l_1} = 4, & \beta_{l_2} = 1, \\ R_{c_m} = diag\{3, 0.25\}, & \alpha_{m_1} = 0.24, & \alpha_{m_2} = 0.6, & \beta_{m_1} = 1.6, & \beta_{m_2} = 0.8, \\ K_c = diag\{0.1, 0.1\}, & \alpha_{\sigma_1} = 0.25, & \alpha_{\sigma_2} = 0.4, & \beta_{\sigma_1} = 4, & \beta_{\sigma_2} = 2, \\ K_\sigma = diag\{0.4, 0.3\}, & & & & \end{array}$$

Experimental results

The results for the time-based routine without the end-effector are shown in Figure 6.8. The saturated control with integral action exhibits better performance than the control without integral action. As expected, the steady state error can be diminished greatly and the oscillations have been eliminated. However, in order to attain the desired position during the first small movement, the control parameters must be set such that the subsequent movements have an overshoot. Each movement reaches a steady state within 7 seconds, but a small steady state error is still present sporadically.

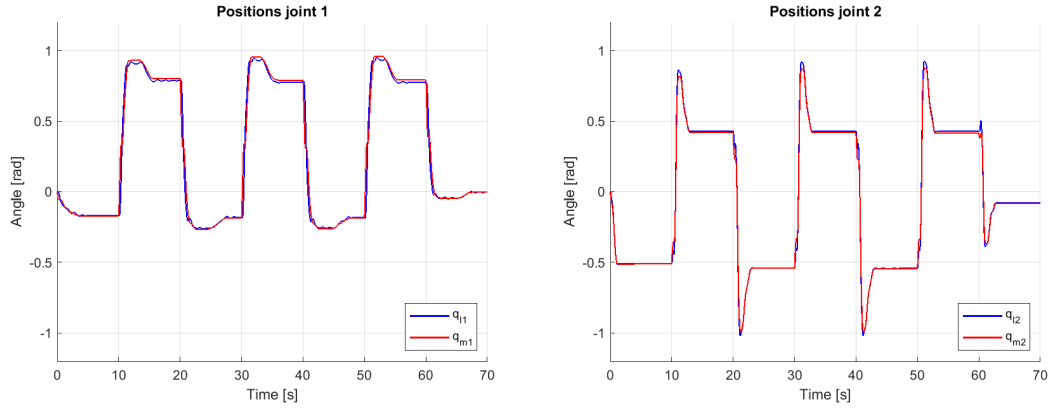

(a) Positions joint 1 (b) Positions joint 2

Figure 6.8: Joint positions for time-based routine

For the first joint, the first movement does not attain its desired position exactly, while there is a an overshoot in the subsequent movements. It can also be observed that the overshoot in the negative movements towards the picking position ($q_pick = (-0.2)$) for the first joint are slightly smaller than the overshoots in the positive movements.

The second joint does attain its desired position in all movements, but shows strong overshoots. These overshoots are partly the result of the high control parameters needed to attain the desired position in the first movement, and partly a side-effect of the strong decelerations in the first joint. The accelerations in the first joint have increased to attain the desired position in the first movement as well, which has lead to larger overshoots in the second joint; this was also shown in the results from Figure 6.4 and 6.6..

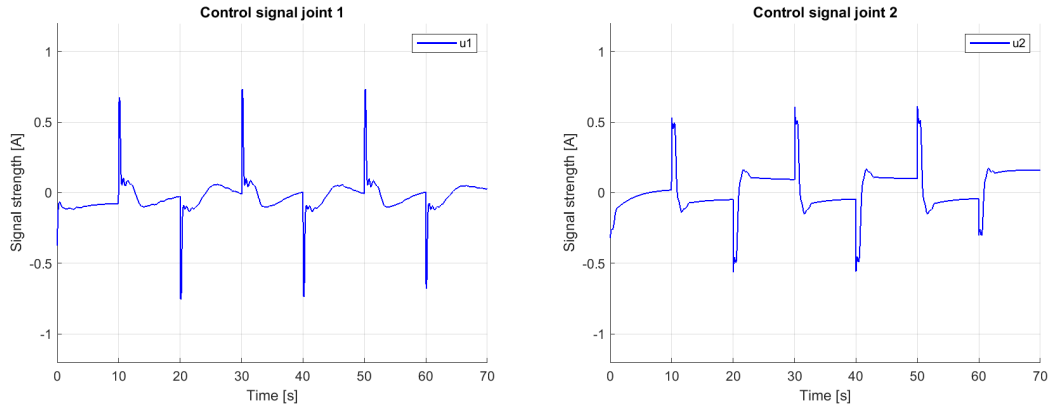

(a) Control signal joint 1 (b) Control signal joint 2

Figure 6.9: Control signals for time-based routine

The impact of the integral action on the control signals in Figure 6.9 is evident as well. The control signal decline into a constant value near zero after the initial peak, but adapts slowly to decrease the steady state error. Figure 6.9 also shows that the steady state error is not eliminated entirely, noticable by the non-constant, non-zero control signals at the end of each movement.

Also note that the highest control signal peak that is achieved does not approach the saturation level by some distance, and the peaks are also lower than in the control law without integral action. Recall that these saturation levels are 0.944[A] and 1.21[A] for joint 1 and 2 respectively, while the peaks are roughly equal to $\alpha_m + \alpha_l$. This can be explained because the u_σ element of the control law is much slower to adapt than the other two elements. Since the current saturation level is divided among the three elements $(\alpha_l, \alpha_m, \alpha_\sigma)$ instead of two, the total control signal remains lower.

In Figure 6.10 it can be seen that the positional error of the end-effector is much smaller than in the controller without integral action, and the oscillations are gone. The first movement just attains the desired maximum error, and the subsequent movements all attain the desired accuracy. The form of the error in each movement

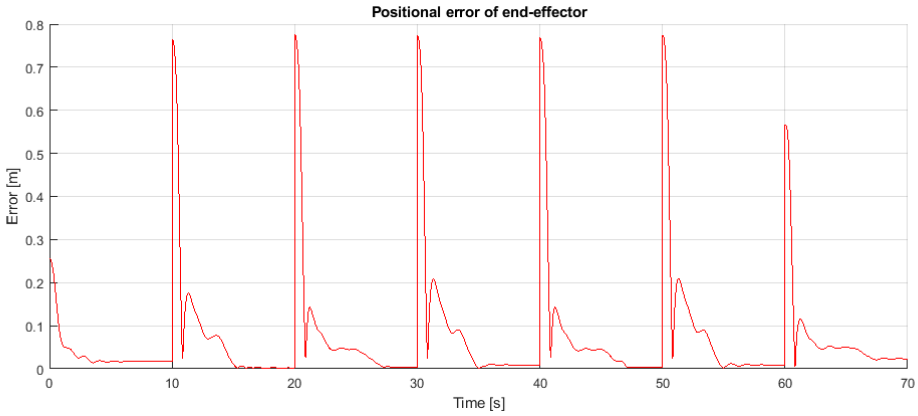

Figure 6.10: Positional error of end-effector

clearly shows the initial error, the overshoot and then the convergence towards the desired position. Also note that the overshoot for every picking movement is slightly smaller than the overshoot for the placing movement.

It can be concluded that the control law that was presented in Section 4.2 is able to attain the desired accuracy that is needed to perform a pick and place routine.

Position-based routine

Now the results for the time-based routine show that the controller can achieve the desired accuracy, the same control parameters will be tested on the position-based routine. The results are shown in Figure 6.11, where three pick and place movements are performed after which the arm returns to its initial position.

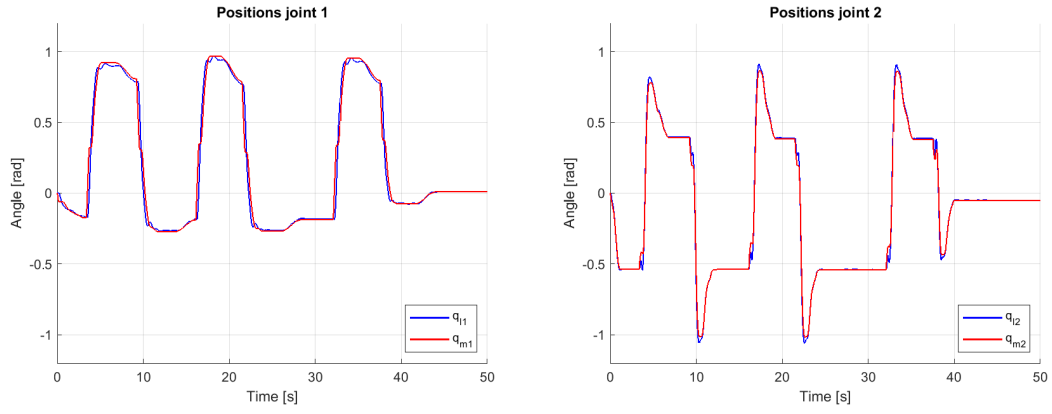

(a) Positions joint 1 (b) Positions joint 2

Figure 6.11: Joint positions for position-based routine

The timing of the movements are somewhat irregular, most noticeably is the lack of movement at 25s. This happened at the 'pick'-position, because the end-effector did not grasp the cup strong enough. Besides this anomaly, the behavior is rather consistent; there is a comparable overshoot with the time-based routine, after convergence the arm immediately moves towards the next position.

The control signals are shown in Figure 6.12. A small difference in the position-based approach is that the σ-term in the controller does not have time to stabilize when the desired position is attained, leading to slightly different control signals. Overall, this has a slightly negative impact one the time to steady-state. The time to steady state stays under 8s and the desired level of accuracy is achieved in every movement.

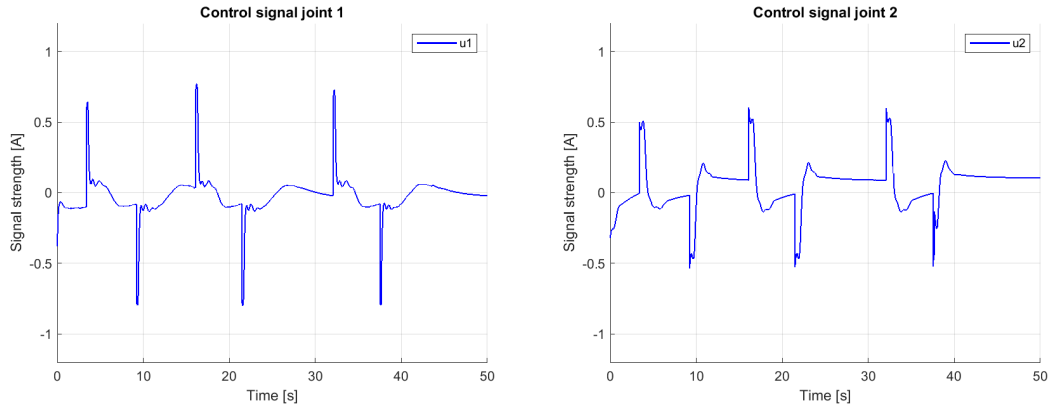

(a) Control signal joint 1 (b) Control signal joint 2

Figure 6.12: Joint positions for time-based routine

The positional error is shown in Figure 6.13. At each movement besides the smaller first and last movements, the position error is very close to zero.

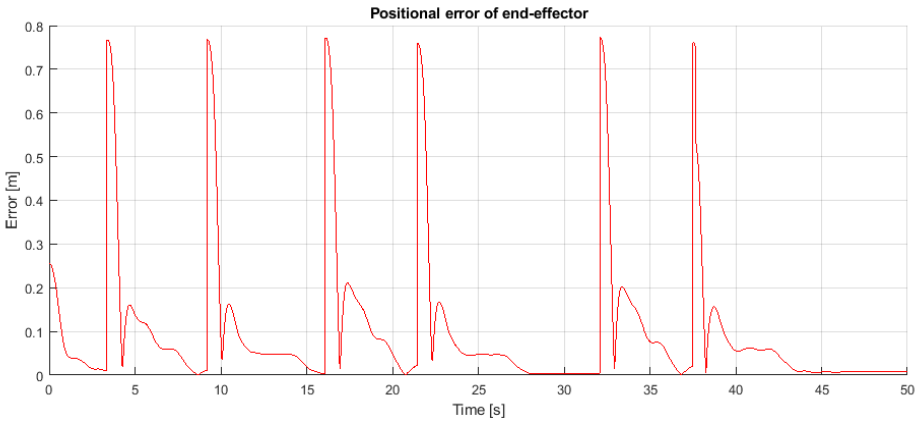

Figure 6.13: Positional error of end-effector

Conclusions

The controller that was tested in this section is a clear improvement when compared to the controller without integral action that was discussed in section 6.2. The integral action nearly eliminates the steady state error in the experiments, and ensures that the end-effector can approach the desired position closely enough to perform the pick and place routine. With the addition of this extra element to the controller, the oscillations due to flexibility are also reduced.

One drawback that can be observed is that in order to adequately reduce the steady state error in all movements, an overshoot occurs in all but the movement to and from the initial position. This can be contributed to a combination of the slow adaptation of the integral action, and the nonlinear friction. The high static friction has a much stronger impact on the small initial movement, because the control signal first needs to overcome a threshold, which is achieved by increasing the control parameters related to u_σ, the integral action. As a result, this integral control on the subsequent movements is stronger than necessary. Finding the right balance to attain the desired position in the initial movement and avoiding very strong overshoots is a rather rigorous task in this experimental setup.

6.4 Parameter testing

To gain some more insight into structure of the saturated control law with integral action ($u = u_l + u_m + u_\sigma$), additional testing was carried out for cases with special control parameter configurations.

Test for $\alpha_l = 0$

The u_l element functions as a damping on the links, which can be used to decrease the oscillations. However, the results from Section 6.2 showed that introducing u_σ also had a positive impact on reducing the oscillations. Here, it will be demonstrated what happens when setting $\alpha_l = 0$, effectively eliminating u_l from the controller.

The following control parameters were recalibrated to enable the best performance. The results are shown in Figure 6.14.

$$R_{c_m} = diag\{10, 5\}, \quad \alpha_{m_1} = 0.3, \quad \alpha_{m_2} = 0.6, \quad \beta_{m_1} = 1.2, \quad \beta_{m_2} = 1,$$
$$K_c = diag\{0.1, 1\}, \quad \alpha_{\sigma_1} = 0.64, \quad \alpha_{\sigma_2} = 0.6, \quad \beta_{\sigma_1} = 1, \quad \beta_{\sigma_2} = 1,$$
$$K_\sigma = diag\{0.5, 0.5\},$$

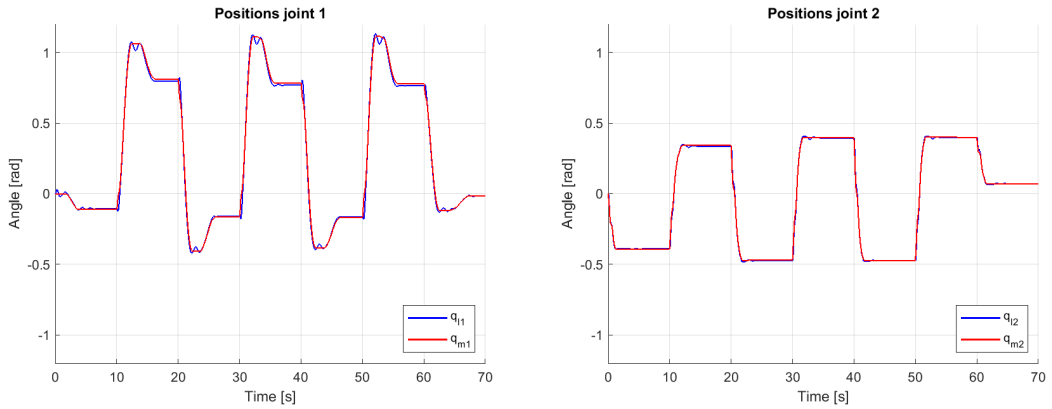

(a) Positions joint 1 (b) Positions joint 2

Figure 6.14: Joint positions for time-based routine with $\alpha_l = 0$

The first joint does not reach its position in the first movement, and has rather large overshoots in the subsequent movements. This is because the movements are not damped as effectively as they were when α_l was non-zero. In spite of these overshoots, the position of the first joint does converge rather well. Also, there are small oscillations in the link during the overshoot.

For the second joint, the first movement does not reach its desired position as well, but there are no overshoots in the subsequent movements. Closer inspection into the graph and data for the joint 1 positions actually shows that the slope during the movements is a bit less steep than in the results of Section **??**. As a

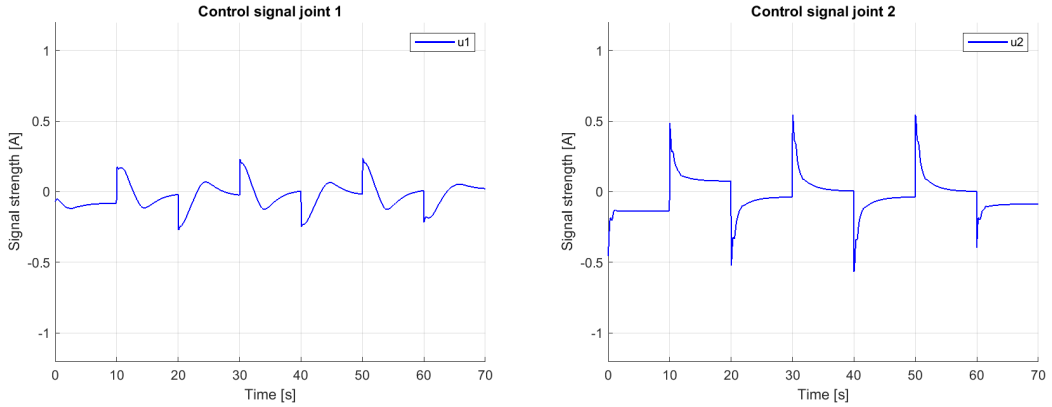

(a) Control signal joint 1 (b) Control signal joint 2

Figure 6.15: Control signals for time-based routine with $\alpha_l = 0$

result, the deceleration in the first joint is decreased, apparently just enough to not result in an overshoot in the second joint. The oscillations in the second link remain very small.

In the experiments without the integral action from Section 6.2, a high α_l was needed to damp the oscillations. It turns out that the α_σ can also do a pretty good job of damping the oscillations, while still reducing the steady state error.

It is worth noting that the control signals (see Figure 6.15) for joint 1 remain rather small, while still resulting in a fast movement. The peaks in the control signal are between 0.20[A] and 0.25[A], while in section 6.3 the peaks were between 0.6[A] and 0.7[A]. This indicates that the motor is sensitive to its input signal when it is small, and that a small increase in control signal (e.g. from 0.12[A] to 0.2[A]) can result in a large increase in velocity. Relating this to the friction, it can be assumed that the friction decreases significantly when the control signal first overcomes the static friction. The increase in velocity is smaller for increase in control signal between 0.25[A] 0.5[A], which indicates a greater increase in friction. The decrease in friction at these lower velocities is called the Stribeck-effect [15].

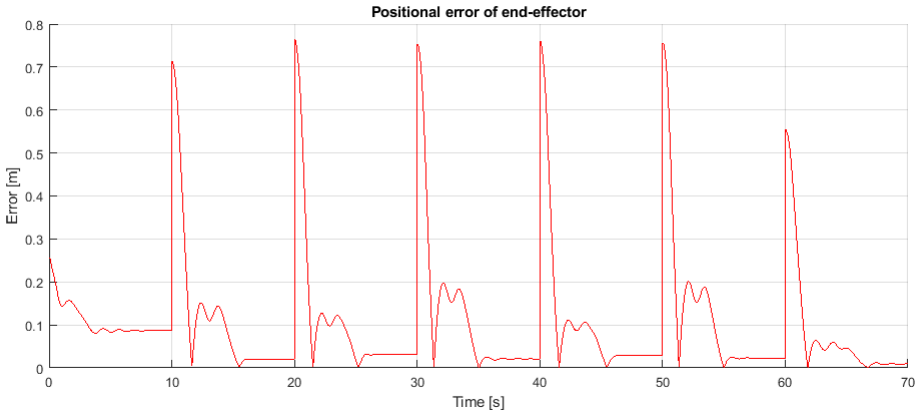

Figure 6.16: Error signal for the case $\alpha_l = 0$

In Figure 6.16, the positional error of the end-effector is shown. The overshoots and oscillations in the first joint are clearly visible, and there is a slightly less accurate convergence of the end-effector position. Comparing these results with the controller from 6.3, it can be concluded that despite the absence of α_l relatively accurate movements can still be attained, but the initial movement is not accurate, and there are some oscillations. Ultimately, the movements are not accurate enough for the pick and place routine.

Test for $\alpha_m = 0$

The u_m element of the controller increases its signal strength when the motor angle is far from its desired position. In this section, the value for the α_m parameter will be set to zero, eliminating u_m from the controller. The remaining control parameter values are given below, and the results are shown in Figure 6.17.

$$R_{c_l} = diag\{10, 10\}, \quad \alpha_{l_1} = 0.3, \quad \alpha_{l_2} = 0.6, \quad \beta_{l_1} = 1, \quad \beta_{l_2} = 1,$$
$$K_\sigma = diag\{0.5, 0.5\}, \quad \alpha_{\sigma_1} = 0.64, \quad \alpha_{\sigma_2} = 0.6, \quad \beta_{\sigma_1} = 1, \quad \beta_{\sigma_2} = 1,$$

Looking at the control parameters, a clear similarity is present between the parameters in the previous test. Furthermore, the results are similar as well, indicating that the u_l and u_m elements of the controller can perform more or less the same function in this case.

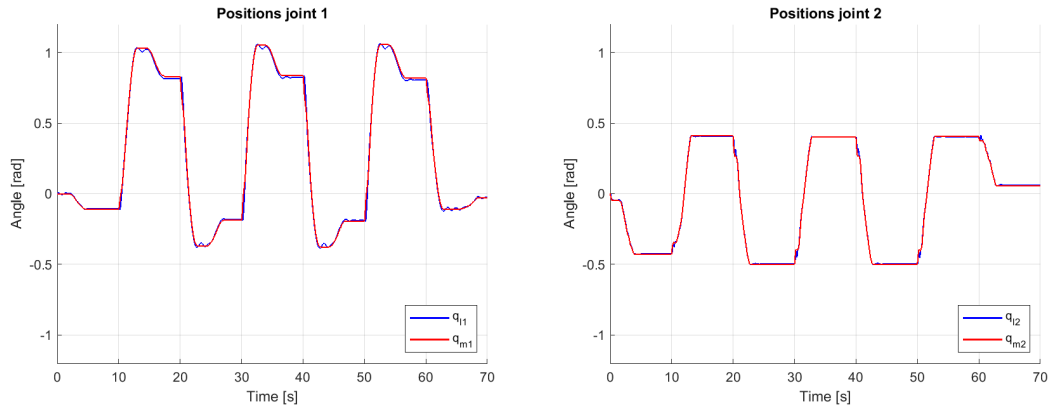

(a) Positions joint 1 (b) Positions joint 2

Figure 6.17: Joint positions for time-based routine for the case $\alpha_m = 0$

The positions for both joints look similar to the case for $\alpha_l = 0$. In the position for joint 1, it is clear that the first movement does not reach its desired position, but the subsequent movement converge rather well. Without the u_m, the positions in the first joint exhibit a slower movement towards the desired position, which does not induce an overshoot in the second joint. For the second joint, the integral action can almost attain a perfect position in every movement. Moreover, the oscillations in the first joint are slightly smaller than in the case $\alpha_l = 0$.

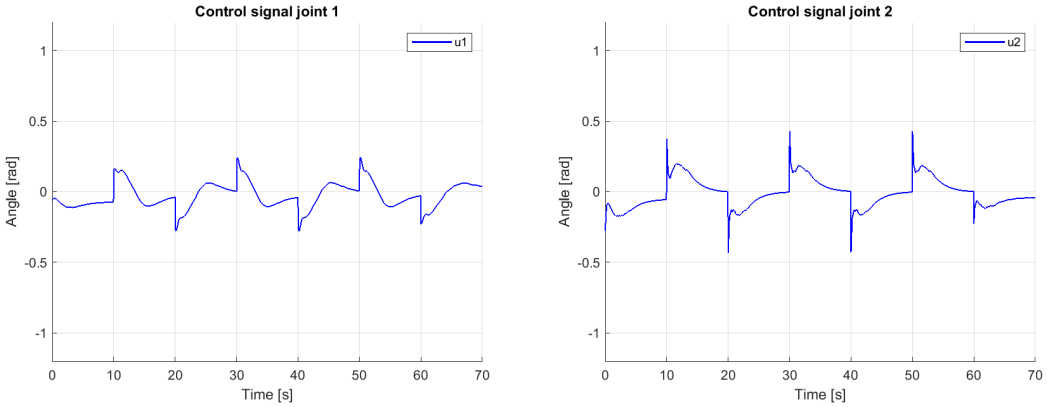

(a) Control signal joint 1 (b) Control signal joint 2

Figure 6.18: Control signals for time-based routine for the case $\alpha_m = 0$

The control signals are shown in Figure 6.18. The difference in the second joint control signals between this case and the case for $\alpha_l = 0$ is due to the difference between the R_{c_l} and R_{c_m} parameters. The second joint value for R_{c_l} is higher than the value for R_{c_m} from the previous test, which results in a stronger damping. This is needed, because the additional damping effect that K_c had in the previous test is not present here.

The positional error is shown in Figure 6.19, and it can be seen that all movements except the initial one converge nicely towards the desired position.

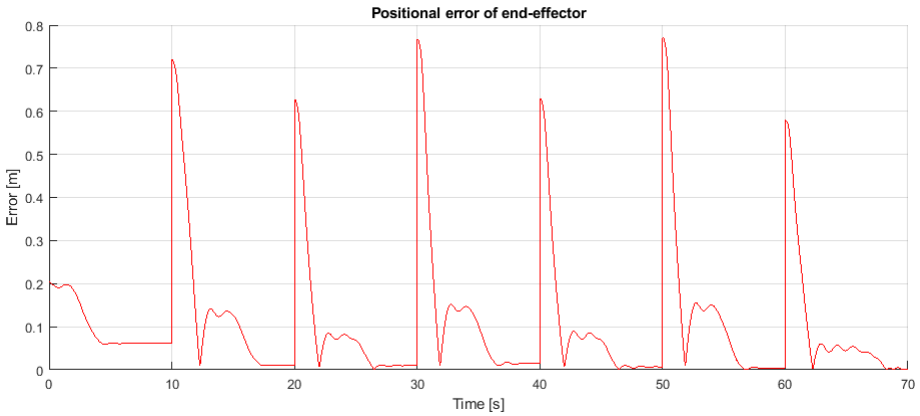

Figure 6.19: Error signal for the case $\alpha_m = 0$

It can be concluded that the performance for $\alpha_l = 0$ is slightly better than the performance when $\alpha_m = 0$. Still, the lack of accuracy in the first movement remains a problem.

Approaching the lower bound for R_{c_l}

Another interesting aspect of the controller is the lower bound that is set on R_{c_l} (see equation (4.4)), which forms a basis for the proof of stability of this controller. In this section, it will be shown what what happens when the values for R_{c_l} approach their lower bound. Using the parameter values for D_l and D_m that were calculated in Section 6.1 (see Table 6.2), this lower bound is identified to be around $diag\{1.6, 5.7\}$.

The following control parameters are set.

$$
\begin{array}{lllll}
R_{c_l} = diag\{4, 10\}, & \alpha_{l_1} = 0.45, & \alpha_{l_2} = 0.2, & \beta_{l_1} = 4, & \beta_{l_2} = 1, \\
R_{c_m} = diag\{3, 0.25\}, & \alpha_{m_1} = 0.24, & \alpha_{m_2} = 0.6, & \beta_{m_1} = 1.7, & \beta_{m_2} = 0.8, \\
K_c = diag\{0.1, 0.1\}, & \alpha_{\sigma_1} = 0.25, & \alpha_{\sigma_2} = 0.4, & \beta_{\sigma_1} = 4, & \beta_{\sigma_2} = 2, \\
K_\sigma = diag\{0.35, 0.3\}, & & & &
\end{array}
$$

Note that all parameters are identical to the ones in Section 6.3, except for R_{c_l}, which is set lower. The results are shown in Figure 6.20.

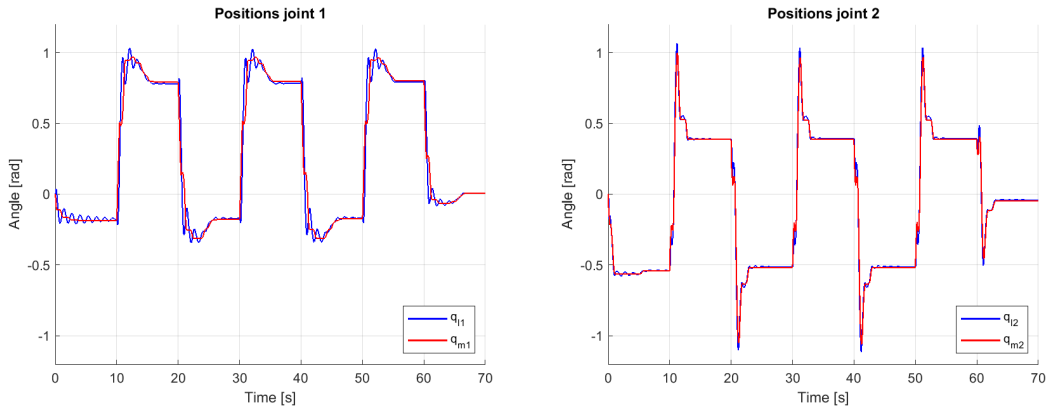

(a) Positions joint 1 (b) Positions joint 2

Figure 6.20: Joint positions for time-based routine for a low R_{c_l}

There are clear oscillations during the overshoots, which are diminished somewhat by the integral action that steadies the arm near the desired position. Again, there are large overshoots in the second joint, which exhibit some oscillations as well. Despite the oscillations, the movements in both the first and second joint do converge to their desired positions.

The effect of the low R_{c_l} is also clear in the spiky control signals, which are shown in Figure 6.21. The control signal for the second joint has extremely large peaks when compared to the previous results. This is also a clear consequence of the low R_{c_l}, because the damping on the control signal is much less.

In Figure 6.22 the positional error of the nd-effector is shown, which clearly show the oscillation, and the convergence to the desired position.

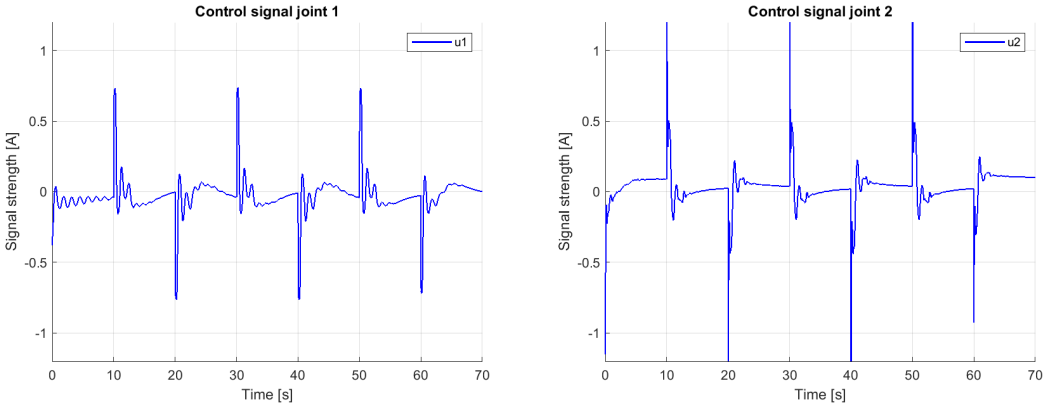

(a) Control signal joint 1 (b) Control signal joint 2

Figure 6.21: Control signals for time-based routine for a low R_{c_l}

It is evident that the value of R_{c_l} is important to the performance of the controller. To damp the oscillations and maintain a smooth movement, a relatively high R_{c_l} is needed, higher than the theoretical lower bound. On the other hand, a very high R_{c_l} will damp the control signal for u_l too much, and diminishes its impact. For the second joint, this effect is less strong, because the second link is less prone to oscillations, which was shown in the previous sections.

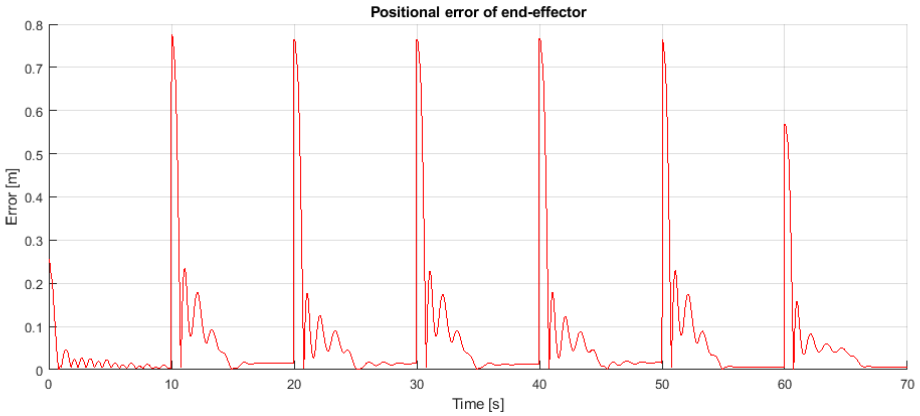

Figure 6.22: Error signal for a low R_{c_l}

Chapter 7

Conclusions

In this research, two naturally saturated control laws that only use position measurements were analyzed, and their performance was tested using a pick and place experiment.

The experiments that were performed gave more insight into the performance of the controllers, and practical issues such as motor asymmetry and the Stribeck-effect were identified.

Additionally, an attempt was made to determine better damping parameters, improving the simulation model to better represent the actual behavior of the robotic arm. Also, special effort was made to create more insight into the structure of both controllers, and additional experiments were performed to determine and explain the behavior of specific control parameters.

On the control laws

The control law that was presented in Section 4.1 and tested in Section 6.2, shows a clear trade-off between reaching the desired position with strong oscillations and minimizing the oscillations but inducing a significant steady state error. When the oscillations are minimized, the end-effector of the arm was unable to attain its desired accuracy due to the steady state error. Configuring the control parameters to reduce the steady state error leads to strong oscillations, which inhibits the possibilities for adequate picking and placing of objects.

For these reasons, the saturated control law without integral action is not suitable for a pick and place routine.

With the control law that was presented in Section 4.2, it is possible to achieve more accurate movements in both directions, for different reference positions. The difficulties with attaining the first small movement, an angular displacement of 0.2[rad], can be attributed to the large friction forces at these slower velocities. The overshoot that occurs in subsequent movement is a consequence of needing a larger signal for this initial movement. A second consequence of the larger control signal in the first joint, is that the strong deceleration results propagates to the second link, causing an overshoot. However, each movement was able to reach

the desired accuracy in the end-effector to perform the pick and place routine successfully.

On the practical challenges

The most notorious issue that made the experiments more difficult, was the nonlinear friction. For the first joint for instance, a large static friction causes the motor to remain still for control signals between $-0.12[A] < u < 0.10[A]$. This also shows the asymmetrical aspect directly: the movements with a negative control signal were more difficult than the movements with a positive control signal.

Additionally, after the static friction is overcome, the velocity increases greatly for slightly higher control signals, until values of approximately 0.20[A]. Above this value, increasingly higher control signals only lead to slightly higher velocities. This relation between control signal and velocity can be described by the Stribeck-effect.

In general, determining the appropriate control parameters to obtain the best experimental results was a rather onerous task. The practical issues that come with this specific robotic arm by Quanser proved to be challenging, especially in performing small movements. The high static friction means that a relatively high control signal is needed to achieve even a small movement, and establishing the control parameters that enable an adequate small movement often result in overshoots in the larger movements.

The control laws performed better in the setpoint regulations [19, 5] because the control parameters can then be optimized for one specific movement.

7.1 Future research

First of all, it would be interesting to investigate how nonlinear friction can be implemented in to the model, since its effect is very prominent.

On the other hand, it would be interesting to test these controllers on a robotic arm with different specifications. Especially, this would enable further investigation into how controller performance would change if the static friction is less pronounced, if the motors have a higher saturation point or if they would be slightly less sensitive to differences in low control signals.

Thirdly, the proof for the controller in Section 4.2 only shows local asymptotic stability around the equilibrium point, because it relies on a linearization. Possibilities to proof the stability without the linearization, maybe enabling a proof for global asymptotic stability, should be investigated.

Appendix A

Error calculation

For a two joint planar robotic arm, the position of the end-effector in a Cartesian plane can be calculated using the length l_i of each link and the angle q_i of each link, with $i \in 1, 2$. In Figure A.1, the link angles are denoted by q_1^i.

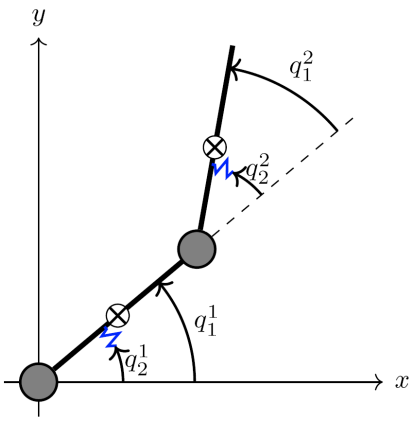

Figure A.1: Schematic representation of the robotic arm, from [12]

Denote the position of the end-effector by (x_e, y_e) and we can calculate

$$\begin{aligned} x_e &= \cos(q_1)l_1 + \cos(q_1 + q_2)l_2 \\ y_e &= \sin(q_1)l_1 + \sin(q_1 + q_2)l_2 \end{aligned} \tag{A.1}$$

Let $q_* = (q_{*_1}, q_{*_2})$ be the desired joint angles, and which can be used to calculate the desired position of the end-effector, given by x_* and y_*, in the same manner. Then, the error between the actual position of the end-effector and the desired position can be calculated using the Pythagorean Theorem:

$$error = \sqrt{(x_* - x)^2 + (y_* - y)^2} \tag{A.2}$$

Bibliography

[1] S. Akella et al. "Parts Feeding on a Conveyor with a One Joint Robot". In: *Algorithmica* 26.3 (2000), pp. 313–344.

[2] A. Albu-Schäffer, C. Ott, and G. Hirzinger. "A unified passivity-based control framework for position, torque and impedance control of flexible joint robots". In: *The international journal of robotics research* 26.1 (2007), pp. 23–39.

[3] K.J. Aström and R.M. Murray. *Feedback systems: an introduction for scientists and engineers*. Princeton university press, 2010.

[4] P. Borja, R. Cisneros, and R. Ortega. "A constructive procedure for energy shaping of port—Hamiltonian systems". In: *Automatica* 72 (2016), pp. 230–234.

[5] P. Borja, T. Wesselink, and J.M.A. Scherpen. "Saturated control without velocity measurements for planar robots with flexible joints". In: *arXiv preprint arXiv:1812.08257* (2018).

[6] D.K. Campbell. "Nonlinear science". In: *Los Alamos Science* 15 (1987), pp. 218–262.

[7] A. De Luca and W.J. Book. "Robots with flexible elements". In: *Springer handbook of robotics*. Ed. by Bruno Siciliano and Oussama Khatib. Springer, 2016. Chap. 11, pp. 243–282.

[8] D.A. Dirksz. *Robust energy-and power-based control design: Port-Hamiltonian and Brayton-Moser systems*. [Sn], 2011.

[9] D.A. Dirksz, J.M.A. Scherpen, and R. Ortega. "Interconnection and Damping Assignment Passivity-Based Control for Port-Hamiltonian mechanical systems with only position measurements". In: *2008 47th IEEE Conference on Decision and Control*. IEEE. 2008, pp. 4957–4962.

[10] V. Duindam et al. *Modeling and control of complex physical systems: the port-Hamiltonian approach*. Springer Science & Business Media, 2009.

[11] K. Fujimoto and T. Sugie. "Canonical transformation and stabilization of generalized Hamiltonian systems". In: *Systems & Control Letters* 42.3 (2001), pp. 217–227.

[12] H. Jardón-Kojakhmetov, M. Muñoz-Arias, and J.M.A. Scherpen. "Model reduction of a flexible-joint robot: a Port-Hamiltonian approach". In: *IFAC-PapersOnLine* 49.18 (2016), pp. 832–837.

[13] H.K. Khalil. *Nonlinear systems, 3rd edition*. New Jersey: Prentice-Hall, Inc, 2002.

[14] R. Miranda-Colorado, L.T. Aguilar, and J. Moreno-Valenzuela. "A model-based velocity controller for chaotization of flexible joint robot manipulators: Synthesis, analysis, and experimental evaluations". In: *International Journal of Advanced Robotic Systems* 15.5 (2018), pp. 1–15.

[15] H. Olsson et al. "Friction models and friction compensation". In: *Eur. J. Control* 4.3 (1998), pp. 176–195.

[16] A.J. van der Schaft. *L2-gain and passivity techniques in nonlinear control*. Vol. 2. Springer, 2000.

[17] B. Siciliano and O. Khatib. *Springer handbook of robotics*. Springer, 2016.

[18] M.W. Spong. "Modeling and control of elastic joint robots". In: *Journal of dynamic systems, measurement, and control* 109.4 (1987), pp. 310–318.

[19] T. Wesselink. "Non-linear saturated control without velocity measurements for planar, flexible-joint manipulators". Research Project, Industrial Engineering and Management. University of Groningen, 2018.

[20] G.R. Widmann and S. Ahmad. "Control of industrial robots with flexible joints". In: *Robotics and Automation. Proceedings. 1987 IEEE International Conference on*. Vol. 4. IEEE. 1987, pp. 1561–1566.

[21] J.C. Willems. "Dissipative dynamical systems part II: Linear systems with quadratic supply rates". In: *Archive for rational mechanics and analysis* 45.5 (1972), pp. 352–393.